Title:

Evolution of hind limb morphology of Titanosauriformes (Dinosauria, Sauropoda) analyzed via 3D Geometric Morphometrics reveals wide-gauge posture as an exaptation for gigantism.

Abstract

The sauropod hind limb was the main support that allowed their gigantic body masses and a wide range of dynamic stability adaptations. It was closely related to the position of the centre of masses of their multi-ton barrel-shaped bodies, and experienced one of the most noticeable posture changes during macronarian evolution. Deeply branched macronarians achieved increasingly arched hind limbs in what is known as wide-gauge posture. However, it is not clear if this evolutionary trend is related to the evolutionary cascade toward gigantism even though some titanosaurians were the largest terrestrial vertebrates that ever existed. We tested evolutionary changes in hind limb morphology in the Macronaria phylogenetic tree by 3D geometric morphometrics. The macronarian hind limb does become progressively more arched toward deeply-branched groups, specifically Saltasauridae. However, there is morphological convergence between different macronarian subclades. Wide-gauge posture does not correlate with changes in body size deeper in the macronarian evolutionary tree, and acted as an exaptation to gigantism. Despite some titanosaurian subclades becoming some of the largest vertebrates, there is a phyletic body size decrease in Macronaria.

Main Text

1. Introduction

Sauropod dinosaurs evolved a distinct body plan that allowed them to reach some of the largest body masses of terrestrial vertebrates (e.g., Bonaparte and Coria, 1993; Carballido et al., 2017; Lacovara et al., 2014; Sander 2013; Sander et al., 2011) by one order of magnitude compared to other vertebrates, including other megaherbivore dinosaurs. Sauropods were dominant herbivorous dinosaurs throughout much of the Mesozoic (Sander, 2013; Sander et al., 2011). Several morphological features can be related to the evolutionary cascade that allowed the acquisition of their colossal sizes, such as the vertebral pneumaticity related to avian-like air sacs, high metabolic rates, cranial morphology, and feeding mechanisms (including the characteristic long necks among several other traits, see Sander 2013). Several features on its appendicular skeleton are related to the evolution of columnar limbs. The mechanical stability

of the columnar limbs allowed them to support their multi-ton body masses (Bates et al., 2016; Lefebvre et al., 2022; Salgado et al., 1997; Sander, 2013; Ullmann et al., 2017).

Previous studies based on sauropod anatomical description, systematics, traditional morphometrics, biomechanics and GMM suggested that there was an important evolutionary trend in the appendicular skeleton toward the acquisition of a stable limb posture known as wide-gauge (Klinkhamer et al., 2019; Lefebvre et al., 2022; Salgado et al., 1997; Sander, 2013; Ullmann et al., 2017; Upchurch et al., 2004; Voegele et al., 2021; Wilson and Carrano, 1999; Wilson, 2002). This feature appears among deeply-branched Neosauropoda, in particular, among titanosauriforms, which exhibit a progressively arched limb posture (Salgado et al., 1997; Upchurch et al., 2004; Voegele et al., 2021; Wilson and Carrano, 1999; Wilson, 2002). The wide stance may enable enhanced lateral stability during locomotion allowing them to adapt to a range of new geographic and ecological niches (Mannion and Upchurch, 2010; Ullmann et al., 2017). However, the widening of the body in Titanosauriformes and the acquisition of the wide-gauge stance is still poorly understood. Although the arched limbs and wider postures appeared in the largest sauropods among Titanosauriformes (Bates et al., 2016; Henderson, 2006; Ullmann et al., 2017; Wilson and Carrano, 1999) these features may at least be acquired independently among both small and large titanosauriforms of different subclades (Henderson 2006; Bates et al. 2016). Limb posture may have been related to achieving greater ranges of ecological niches though biomechanical stability rather than body size increases alone (Bates et al., 2016; Henderson, 2006; Ullmann et al., 2017). The study of the hind limb through 2D and 3D geometric morphometrics (GMM) allows us to analyze complex morphological changes across the titanosauriformes phylogeny (e.g., Lefebvre et al., 2022, Ullmann et al., 2017). Here we will use 3D-digitized and reconstructed titanosauriform hind limbs (Table 1, see also Fig. 1) to test whether there is a relationship between wider hind limb posture (as the hind limbs are the main weight support of the sauropod body, see Bates et al. 2016) and their body size (as proxied by the hind limb size). We will also test for potential morphological convergence between different titanosauriform subclades regardless of their body size. The analysis presented here can be seen as an expansion of the Lefebvre et al. (2022) study on sauropod limb evolution as we analyze a sample comprised mostly of Late Cretaceous Lithostrotian sauropods (their study included a broad diversity of sauropodomorph taxa including several titanosaurs).

2. Results

2.1. Titanosauriformes Morphospace Occupation

A Principal Component Analysis (PCA) was performed to generate an occupation morphospace, obtaining a total of 16 shape Principal Components (after Anderson's χ test; PC from now on). The first six PCs accounted for 78.3% of the cumulative morphological variation (Table 2). The non-parametric Kruskal-Wallis test shows that no single shape variable reports significant differences among sauropod subclades (Table 3 and 4). Here we only comment on the results of the first three shape PCs (>50% of the cumulative variance) due to space limitations, but a full description and visualization of the complete PCA and phylomorphospace projections can be found in Appendix S3.

PC1 (summarizing 29.92% of the total variance; Fig. 2a-b) is associated with characters describing the orientation and compression of the femoral shaft, the length of the distal femoral condyles, the orientation of the fourth trochanter, and the length and width of the zeugopod

bones (Fig. 2c). Non-titanosaurian macronarians occupy negative values, whereas non-lithostrotian titanosaurs are distributed between weakly negative (e.g., *Bonatitan*) and positive PC1 values (Fig. 4b). Lithostrotian titanosaurs occupy a wide range of values, with *Aeolosaurus*, the specimens of Colossosauria and *Lirainosaurus* clustering at negative PC1 values (however, *Ampelosaurus* occupies negative PC1 values approaching zero; Fig. 2b). Most of the non-saltasaurid, non-colossosaur, non-lirainosaurine and non-aeolosaurine lithostrotians are broadly distributed in the morphospace between negative and positive values, with *Bonitasaura* occupying the farthest negative PC1 values and overlapping with Colossosauria and Lirainosaurinae (Fig. 2b). The highest positive PC1 values are occupied by saltasaurids (i.e., *Saltasaurus* and *Neuquensaurus*) (Fig. 2b). There is a trend from non-titanosaurian macronarians at negative values to the titanosaurian node at weakly negative values (Fig. 2b). In this PC1, the Titanosauria node splits near a zero score, with *Lohuecotitan* occupying weakly positive PC1 values near a zero score [in recent phylogenetic analyses, *Lohuecotitan* has been recovered as a member of Lithostrotia (Díez Díaz et al., 2020; Navarro et al., 2022)], but other deeply nested titanosaurs occupy positive scores in PC1 (Fig. 2b). The trend toward positive values follows with several other deeply nested lithostrotians. However, both Colossosauria and the two analysed members of Lirainosaurinae fall into negative PC1 values (Lirainosaurinae was not recovered as a monophyletic group in our current topology; Fig. 2b). There are no significant differences between the different sauropod subclades in this PC (Appendix S4).

PC2 (summarizing 14.83% of the variance; Fig. 3a-b) is associated with characters describing the orientation of the femoral shaft; the length and orientation of the femur proximal end; the length, width and orientation of the distal femoral condyles; the orientation of the tibial shaft; the length and orientation of the cnemial crest; the length, width and orientation of the tibial distal end; the orientation of the tibial ascending process; the orientation of the fibular shaft and fibular anterior crest (Fig. 3c). Both the early branching macronarian *Oceanotitan* - a possible member of Somphospondyli (Mocho et al., 2019) - and the euhelopodid somphospondyli *Euhelopus* occupy positive and negative values near a zero score, whereas the early-diverging somphospondylan *Ligabuesaurus* is distributed at slightly more positive PC2 values than *Oceanotitan* (Fig. 3b). However, there is no clear pattern among the titanosaurian subclade morphospace (Fig. 3a) or the phylomorphospace (Fig. 3b) among progressively deeply branching titanosauriforms. The saltasaurids and *Aeolosaurus* occupy positive PC2 scores (Fig. 3b) showing some overlap with Colossosauria at weakly positive values of PC2 (Fig. 3b). Lirainosaurines and colossosaurians are distributed at weakly negative to positive values in PC2 (Fig. 3b). However, non-saltasaurid, non-aeolosaurini, non-colossosaur, and non-lithostrotian titanosaurs are broadly distributed across the morphospace; most of them between negative values (i.e. *Dreadnoughtus*) and positive PC2 values (i.e *Jainosaurus*, *Antarctosaurus*) (Fig. 3a-b). The hind limb occupation of the titanosaur *Dreadnoughtus* at strongly negative PC2 values is noteworthy (Fig. 3a-b). The Mann-Whitney's U test found no significant differences in the PC2 in any of the pairwise comparisons (Appendix S4).

Finally, PC3 (summarizing 11.61% of the variance; Fig. 3a-b, 4a-b) is related to characters describing the orientation of the femoral shaft and head; the length of the femoral lateral bulge; the location and orientation of the fourth trochanter; the orientation of the distal femoral condyles; the length and orientation of the tibial cnemial crest; the length of the tibial distal end; the length of the tibial ascending process; and the length and morphology of the fibula (Fig. 4c). *Oceanotitan* and *Euhelopus* were plotted toward progressively more positive values (Fig. 4a) and the node was estimated at slightly more negative values of PC3 than *Euhelopus* (Fig. 4b). *Ligabuesaurus* occupies positive values of PC3 closer to zero than early branching titanosauriforms (Fig. 4a). In the phylomorphospace, there is a trend from positive values to

negative values of PC3 (Fig. 4b) from more basally branching titanosauriforms to more deeply nested ones. Non-lithostrotian titanosaurs occupy negative PC3 values but the non-saltasaurid, non-lirainosaurine and non-colossosaurian lithostrotians trends towards positive PC3 values (Fig. 4a-b), whereas Lirainosaurinae, Colossosauria and Saltasauridae occupy negative values of PC3 (Fig. 4a-b). Colossosauria, Saltasauridae and *Lirainosaurus*, the most deeply-branched representatives of Lirainosaurinae according to our phylogenetic hypothesis, plotted toward increasingly more negative PC3values (Fig. 4a-b). *Magyarosaurus* is the only lithostrotian occupying high positive values, clearly separate from all other sauropods (Fig. 4a-b). The pair-wise Mann-Whitney's U test found no significant differences between sauropod subclades in this PC (Appendix S4).

2.2. Size distribution

There is a trend in hind limb centroid size distribution from large, non-titanosaurian macronarians in the Early Cretaceous (e.g., *Euhelopus*) to small, deeply nested lithostrotian titanosaurs in the Late Cretaceous (Fig. 5). This trend coincides with the morphospace occupation recovered by PC1 (early-branching and larger non-titanosaurian macronarians among negative PC1 values and progressively more deeply nested and smaller titanosaurs toward positive PC1 values (Fig. 5). The smallest lithostrotians are concentrated at deeply branching nodes, including the Ibero-Armorican lirainosaurines, *Bonatitan reigi*, *Magyarosaurus* spp. and members of Saltasaurinae (Fig. 5).

However, the RMA models found no significant correlation between the shape variables and the log-transformed centroid size (Table 6, see Fig. 6 and Appendix S3). The PC1 model (r^2 = 0.105, p-value= 0.204; Fig. 6a) found negative allometry but no significant correlation and the percentage of variance explained by hind limb size differences was small. Almost all of the RMA found a negative relationship, except for several sub-sampled RMA models like the PC2 against log-transformed centroid size for the sample of lithostrotian titanosaurs only (Fig. 6b). None of the RMA models for the sub-samples found a significant correlation (see Appendix S3).

2.3. Phylogenetic trends

Pagel's lambda (λ) estimation shows a significative phylogenetic signal in log-transformed hind limb centroid size (λ = 0.982), and PC1 (λ = 0.715), PC3 (λ = 0.760), PC5 (λ = 0.778) and PC6 (λ = 0.697) therefore exhibiting a trend in the evolution of Titanosauriformes (Table 7). We estimated ancestral characters (ACEs) using log-transformed hind limb centroid size and those shape variables (the PCs) that exhibit a significant signal during the evolution of Titanosauriformes and tested for a directionality or trend (Fig. 7). The resulting tests recover significant trends toward a decrease in hind limb size across all titanosauriform subclades, positive PC1 values up to Somphospondyli Titanosauriformes, and negative PC3 values across all titanosauriform subclades (electronic Appendix S4, table S4.8, S4.9, S4.10).

3. Discussion

3.1. Hind limb morphological convergence in Titanosauriformes

Analysis of the shape variables extracted by PCA on the Procrustes coordinates of the sauropod taxa reveals a large overlap between the different titanosauriform subclades, in particular within Titanosauria (e.g., Fig. 2-4), across all the resulting shape PCs. Both the non-parametric tests on

the hind limb shape variables and the size, and the phylogenetic ANOVA accounting for the time-calibrated supertree topology, suggest the lack of sufficient and significant morphological differences between the different titanosauriform subclades studied in this analysis. Based on the lack of significant phylogenetic differences and the presence of morphological similarities, the evolutionary pattern observed for the titanosaurian hind limb may be explained by convergent evolution, consistent with previous analyses (Lefebvre et al., 2022; Páramo, 2020; Páramo et al., 2020; Ullmann et al., 2017).

Considering the analysed sample, the acquisition of wide-gauge locomotion would be the main source of hind limb morphological variability in titanosaurian sauropods (Fig. 2, 5) and possesses a significative phylogenetic signal. The trend toward a more arched limb posture persists in the more deeply nested titanosaurs. *Oceanotitan dantasi*, a possible representative of Somphospondyli, exhibits a columnar hind limb characterized by no deflection of the femoral head with regard to the tibial condyle (though some titanosauriforms exhibits this feature, see Royo-Torres, 2009), and a straight and long, lateromedially-narrow zeugopod with few anterior rotations of the fibula (Fig. 2). In contrast, the more deeply branching titanosauriforms exhibit the typical titanosaurian hind limb configuration with a more arched posture, lateromedially more robust femora, and increased medial or proximo-medial deflection of the femoral head. Distally, the hind limb exhibits a slight rotation of the femoral distal ends, and increasingly lateromedially robust zeugopods. The robust zeugopod elements are the only resemblance to *O. dantasi* as our outgroup (e.g., Fig. 2). The highest positive PC1 (Fig. 6) values correlate with several hyper-robust taxa of different titanosaur subclades that exhibit lateromedially and anteroposteriorly wide stylopods and zeugopods. In these taxa, the zeugopod bones are extremely shorter proximodistally, extremely arched with a predominance of tibiae characterized by short cnemial crests but somewhat rotated, interlocking with anteriorly deflected and robust fibulae as in the saltasaurine *Saltasaurus loricatus*, the lithostrotian *Magyarosaurus* spp. and the possible non-lithostrotian titanosaur *Dreadnoughtus schrani* (based on the super-tree: Fig. 2,5). The acquisition of this particular morphology is correlated with the development of gigantism within Titanosauria (Carrano, 2005; Lefebvre et al., 2022; Ullmann et al., 2017), at least when analysing early branching members of Lithostrotia. However, specimens occupying higher PC1 values exhibit the most hyper-robust and arched hind limbs including representatives of the smallest lithostrotians and the largest non-lithostrotian titanosaur studied (Fig. 5). The analyses of evolutionary trends presented here reveal that the trend toward titanosauriform gigantism shifted toward adaptation to dwarfism in some lithostrotian titanosaurs like *Magyarosaurus* and *Neuquensaurus* (see discussion on hind limb size variability below). In general, the results obtained here confirm the previously proposed trend toward the acquisition of robust and arched hind limbs in Titanosauria (Fig. 7). Nevertheless, once hind limb mechanical stability was acquired (following e.g., Ullmann et al., 2017) the increasingly arched and robust morphologies established within Titanosauria cannot be fully related to an increase in body mass (Fig. 6a) and are better explained as convergence between different subclades (Figs. 2 and 6, see evolutionary trend breakdown in Table 7). Saltasaurine lithostrotians are characterized by this type of extreme morphology, with hyper-robust limb bones. Even large saltasaurid sauropods like *Opisthocoelicaudia skarzyinski* exhibit this type of hind limb (Borsuk-Bialynicka, 1977). However, this morphology is not exclusive of saltasaurids, since other titanosaurs exhibit homoplastic hyper-robust and arched hind limbs (i.e., *Dreadnoughtus* and *Magyarosaurus*). This progressively arched limb was probably hard-coded in the macronarian bauplan and, after the somphospondylan stable posture was acquired, was still present but relatable to a significant variability of biomechanical adaptations (Voegele et al., 2021) as our analyses suggest. Despite biomechanical diversity associated with hind limb morphology is still unclear, several studies point out that morphological differences in the fore limb elongation in sauropods may be related to different feeding niche capabilities (Bates et al.,

2016; Upchurch et al., 2021; Vidal et al., 2020; Voegele et al., 2020), including discussion on possible bipedal/tripodial rearing abilities that are much more developed, particularly in sauropods with an hyper-robust of hind limb (Upchurch et al., 2021). Interestingly, *Dreadnoughtus* exhibits this hyper-robust hind limb with subequal autopodial lengths and a wedged sacrum (Vidal et al., 2020; Voegele et al., 2021), an anteriorly placed body Centre of Masses (CoM; Bates et al., 2016) and possibly high browsing feeding capabilities (e.g., Vidal et al., 2020). While the small saltasaurids in this study exhibit short necks, stout bodies and a posteriorly placed CoM (Bates et al., 2016) the pneumaticity of some saltasaurid tails (Upchurch et al., 2021; Zurriaguz and Cerda, 2017) may suggest the possibility of a more anterior location of the CoM. It is possible that the acquisition of a hyper-robust and arched hind limb morphology is related to improved skeletal support in high browsing and extremely large sauropods like *Dreadnoughtus*, which in combination with their size and neck dorsiflexion capabilities (e.g., Vidal et al., 2020) allowed them to feed in a high niche stratification, independent of the acquisition of rearing capabilities.

Although PC2 does not provide a phylogenetic signal for the titanosaurian evolution, it reveals significant differences among smaller titanosaurian taxa with robust hind limbs and especially hyper-robust zeugopodia (Fig. 3), like *Magyarosaurus* and the saltasaurines *Neuquensaurus* and *Saltasaurus*, which can be related to different roles in the necessary mechanical stability for rearing capabilities (following Upchurch et al., 2021). *Magyarosaurus*, *Neuquensaurus* and *Saltasaurus* occupy increasingly positive PC2 values (Fig. 3). *Magyarosaurus* exhibits a short zeugopod in which the tibia is slightly laterally rotated, the cnemial crest is laterally projected and the fibula is slightly sigmoidal with its proximal third displaying an anterior projection and a medially deflected anterolateral crest. Saltasaurines exhibit an extreme condition characterized by short and robust zeugopods. Members of this clade show laterally rotated tibiae with posteriorly deflected distal ends, and sigmoidal fibulae that articulate in an oblique position with the anteriorly projected proximal third and anteriorly placed lateral crest. Additionally, this anatomical fibular configuration produces a more anterior displacement of the distal attachment of the *M. iliofibularis* and a probable different distribution of the stress as the main beam of the shafts is rotated from the hind limb trunk, for which previous myological studies suggest that there is no evident body size/phylogenetic pattern (Voegele et al., 2021). In contrast, *Dreadnoughtus* exhibits a slightly arched hind limb posture with a robust zeugopod, a medially deflected cnemial crest of the tibia and a sigmoidal fibula that is slightly posteriorly deflected, and it is projected at negative PC2 (Fig. 3). In this taxon, the fibula, although sigmoidal, articulates in a mostly straight anatomical position with the particularly robust tibia. The differences among robust hind limb titanosaurian morphologies may suggest that their convergence is due to other sources of variation (i.e., different biomechanical adaptations). It is also important to note that all the lithostrotian titanosaurs that exhibit a slightly rotated fibula, whether sigmoid or not, and extremely arched hind limb morphology independent of their size, exhibit femora with reduced fibular epicondyles (after Otero et al., 2020).

Previous studies also pointed to the distinct morphology of the members of Colossosauria, especially in their extremely elongate and gracile zeugopod (González Riga et al., 2018; Páramo et al., 2020). Here we found a distinctive plotting for the rinconsaur hind limb of *Muyelensaurus* and *Mendozasaurus*, often overlapping with *Aeolosaurus*, as in the PC1 and PC3 morphospaces (Figs. 2-4). It is especially relevant that these specimens occupy distinctive PC1 and PC3 scores within Rinconsauria/Colossosauria, which exhibit a signal regarding titanosaurian evolution and corresponding to a specific lineage of this titanosaurian subclade. In addition, the phylomorphospaces indicate that some lithostrotians shift away from the main early-branching lithostrotian area of the morphospace towards a straighter, elongated hind limb convergent with non-titanosaurian macronarians (Fig 2a-b, Fig. 4a-b). In the case of *Aeolosaurus* the phylomorphospace produces a long, branched and wide morphospace occupation among

titanosaurs (Figs. 2-4) as the whole titanosaurian clade re-occupies an entirely new area of the morphospace. Representatives of this group exhibit extremely distinct morphologies, with *Aeolosaurus* and *Antarctosaurus* often much more similar to the early branching non-titanosaurian titanosauriformes than to other deeply-branched titanosaurs (e.g., Fig. 2b, 4b). Colossosauria includes several of the largest titanosaurs ever known (Carballido et al., 2017; González Riga et al., 2019) as well as some of the smallest lithostrotian titanosaurs in South America that are placed within Rinconsauria, which has been recently recovered as an early branching lineage of Colossosauria (Carballido et al., 2017; González Riga et al., 2019). Additionally, some recent phylogenetic hypotheses recovered the aeolosaurine lithostrotians as deeply branching rinconsaurs as well (Carballido et al., 2017; Silva Junior et al., 2022). Whether the appendicular skeleton of Aeolosaurini and Colossosauria exhibits morphological convergence between these two different lithostrotian subclades or they represent the same morphological trend within the same lineage of specialization is still unknown. This depends on whether the latter phylogenetic hypotheses including Aeolosaurini within Colossosauria are accepted as valid. It is important to note that despite the small to medium size of *Muyelensaurus* and *Aeolosaurus*, *Mendozasaurus* can be considered a large sauropod and it exhibits morphological differences from other large sauropods in our sample (i.e., the titanosaurs *Dreadnoughtus* and *Jainosaurus* or the non-titanosaurian somphospondylan *Ligabuesaurus*), similar to previous analyses of separate specimens (Páramo et al., 2020). *Antarctosaurus* seems to be the only large non-colossocaurian titanosaur that shares a similar morphospace with the members of Colossosauria analysed here (i.e., PC1-PC3, Figs. 2-4). The inclusion of hind limb elements of other members of this clade (i.e., *Patagotitan*, *Epachthosaurus*) in future analyses might shed light on this morphological pattern, as the zeugopod elements of several of these taxa resemble those of other non-colossosaur titanosaurs (e.g., *Dreadnoughtus* and *Patagotitan*; see also *Argentinosaurus* in Páramo et al. 2020). Also, *Aeolosaurus* exhibits a different morphology from other post-early Coniacian lithostrotians titanosaurs, thus producing a widening of the occupied morphospace (Fig. 7b-c).

Despite these small differences in the hind limb morphology in key features that may be related to the giant titanosaurian body size, our analyses indicate the great morphological convergence between the different titanosaurian subclades (e.g., *Aeolosaurus* and Colossosauria; or the latter closer to the plesiomorphic morphology of *Euhelopus*, Fig. 2; see also Table 3-4). Also, no significant differences were found in any of the shape variables, either in the pairwise subclade comparisons (Appendix S4), or in the shape PCs that indicate slightly less variance than expected by evolution under Brownian motion (i.e., shape PC1, PC3 in this text, Table 5; shape PC5-6 in Appendix S4).

3.2. Hind limb size evolution

Our results with the current time-calibrated supertree topology indicate that there is a trend in the evolution of titanosaurs towards a decrease in size (Fig. 5 and 7, Tables 5-6). In the light of our current sample, once many of the hind limb features relatable to wide-gauge posture are acquired, there is a phylogenetical trend, close to a pure Brownian motion model, toward an overall decreasing size (log-transformed hind limb centroid size $\lambda = 0.982$), which is consistent with previous results that indicated that lithostrotians (or even all macronarian sauropods) may not follow the Cope's rule (Carrano, 2006; de Souza and Santucci, 2014). This could be due to our current lithostrotian sample as some of the Saltasaurinae or closely related sister taxa (i.e., *Opisthocoelicauda* and *Alamosaurus*, which are usually considered members of a more inclusive clade, Saltasauridae) are also large lithostrotians, especially *Alamosaurus*. However, it is important to note that we also found several key traits in our shape variables (most importantly summarized in PC1 and PC3, 41.53% of the total sample variance between them;

Table 7) that are usually related to the acquisition of gigantism and that exhibit significant signals about titanosaurian evolution. When we tested for a significant correlation between these traits and the log-transformed hind limb centroid size, no significant correlation was found between any of the shape variables and size (Table 4, Fig. 6).

Within Titanosauria, the hind limb arched morphology (increasing wide-gauge posture) does not correspond to the significant trend toward a size decrease observed in this sauropod clade (see Fig. 7, Table 6-7). Large titanosaurs show very different hind limb morphologies. Some lithostrotians exhibit plesiomorphic columnar, slightly arched hind limbs with elongated or even gracile zeugopod elements (*Antarctosaurus*, *Aeolosaurus* or the extremely slender hind limb of the colossosaurs *Mendozasaurus* and *Muyelensaurus*) (Fig. 2), whereas other large titanosaurs (i.e. *Dreadnoughtus)* exhibit an extremely robust hind limb with slightly reduced zeugopods as may be expected from the typical trend toward the acquisition of an arched morphology in Titanosauriformes (Fig. 2a). In this context, it is remarkable that most of the lithostrotians that exhibit extremely arched hind limbs, robust elements and reduced zeugopod elements decrease in size, like *Saltasaurus* or *Magyarosaurus* (Fig. 2, see discussion on morphological convergence above). Our test found that the trend toward this type of hind limb breaks in titanosaurian sauropods, with more variable morphologies and large overlapping of morphospaces whereas the hind limb size decreases (Fig. 7, Table 6-7). Most importantly, PC3 exhibits some of the morphological features that are classically related to wide-gauge arching morphology (e.g.) and our analyses found a significant trend toward increasingly arched hind limbs (Table 8). However, the post-Cenomanian lithostrotians exhibit great morphological variability, with several taxa exhibiting plesiomorphic columnar femora (i.e., *Ampelosaurus*, *Aeolosaurus*, *Magyarosaurus*) and slightly straight zeugopodial elements, with anteriorly expanded tibial proximal ends, and straight non-rotated fibula expanded in the anterior view (Fig. 4,7; see discussion on morphological convergence above). Among these lithostrotians, *Ampelosaurus* and *Aeolosaurus* are medium-sized sauropods, whereas *Magyarosaurus* exhibits both plesiomorphic hind limb morphology and the smallest size. Similarly, the large size variability in the post-early Coniacian cannot be related to the morphological features that are classically associated with the progressively arched morphology (Fig. 7), as discussed before. Therefore, titanosaurs that produce large PC1-PC3 changes at this peak are both moderate-to-large in size, inducing a displacement of the morphospace: (i) toward the plesiomorphic hind limb morphology, plotted in negative PC1 and positive PC3 values (i.e., *Aeolosaurus*) or (ii) toward a morphology intermediate between the main PC1-PC3 typical robust arched titanosaurian hind limb morphology (i.e., *Jainosaurus*) (Fig. 7).

Here it is important to point out that when comparing our results with other lithostrotian titanosaurs not included in the current analysis, similar hind limb posture variability not relatable to hind limb size increases (and therefore body size) is observed. The arched morphology with extremely robust zeugopodial elements exhibited in saltasaurid sauropods (e.g.) is also found in the dwarf non-lithostrotian titanosaur *Diamantinasaurus* (Poropat et al., 2021, 2015). Its tibia shares similarities with those of *Dreadnoughtus* (anteroposteriorly and lateromedially wide proximal end, extremely short and laterally-projected cnemial crest and lateromedially expanded distal end) (Poropat et al., 2015; Ullmann and Lacovara, 2016) whereas the fibula is similar to the slightly straight fibula of *Magyarosaurus*, with a proximally anterior deflection (Poropat et al., 2015; APB direct observation on *Magyarosaurus* sp. specimens). Despite slight differences in the proportion of the zeugopodial elements, the hind limb morphology of *Diamantinasaurus* is similar to those of other small taxa. However, *Rapetosarus* exhibits a completely different lithostrotian hind limb configuration that is more similar to that observed in *Lirainosaurus*. Thus, whereas the fibula is slightly straight with an anteriorly expanded proximal third (Curry Rogers, 2009) as in *Magyarosaurus* and *Diamantinasaurus*, both the tibia and fibula are extremely lateromedially compressed as in

Lirainosaurus or *Muyelensaurus* (APB pers. obs.). Our results are congruent with the observation in other, non-sampled small titanosaurian taxa that exhibit similar morphological variability.

Among large titanosaurs, *Elaltitan* exhibits a (virtually restored) robust femur, a slightly robust and plesiomorphic straight tibia but with a posteriorly rotated distal end, and an extremely sigmoidal and anteriorly projected fibula like those of members of Saltasaurinae but slightly lateromedially narrow compared to the latter (Páramo et al., 2020). Despite some differences, other robust large lithostrotians (i.e., *Dreadnoughtus*) exhibit similar hind limb morphology. However, other large lithostrotians, like *Argentinosaurus*, exhibit a plesiomorphic straight fibula (i.e., Páramo et al., 2020). The hind limb of *Patagotitan* exhibits a less arched posture, with a slightly straighter femur whereas the fibula is robust, sigmoidal and has an anterior expansion of the proximal third (Otero et al., 2020). The stylopodium is not as robust and arched as in *D. schrani* but also exhibit the slightly plesiomorphic titanosaurian straight hind limb, which is also part of the shift toward robust morphology after the earlier branching Colossosauria, such as *Mendozasaurus neguyelap* (Figs. 2 and 4). *Patagotitan* still lacks the extreme medial deflection of the femoral head seen in our PC1 positive and PC3 negative values. *Petrobrasaurus* and *Narambuenatitan* are both large titanosaurs that exhibit similar medial deflection of the femoral head to *Dreadnoughtus*, and in the case of *Narambuenatitan*, even more so than *Saltasaurus* and *Neuquensaurus* (Páramo et al., 2020). However, the tibia of *Petrobrasaurus* is extremely lateromedially narrow as in *Mendozasaurus* (Páramo et al., 2020; APB pers. obs.) instead of the typical robust tibiae of the extremely arched hind limb found in our results (see Fig. 2). Only *Uberabatitan* exhibits a clear morphology like the hind limb morphology found in *Dreadnoughtus* and our positive PC1 scores. Another large titanosaur that exhibits a lateromedially narrow proximal tibial end is *Ruyangosaurus* (Lu et al., 2009). Despite being fragmentary, the femur is straight (with a rounded shaft) and has a tibia with lateromedially narrow proximal end similar to that observed in *Ligabuesaurus* and the members of Colossosauria (which are closely positioned in our analyses) (Figs. 2 and 4). Other more deeply branching lithostrotians either exhibit a hind limb that closely resembles the early-branching Colossosauria or a plesiomorphic tibia as in *Abditosaurus* (Vila et al., 2022). In this taxon, the femur is anteroposteriorly-narrow with a highly eccentric shaft, like other Ibero-Armorican lithostrotians (e.g., *Ampelosaurus*). *Abditosaurus* also preserves an extremely lateromedially narrow tibial proximal end (Vila et al., 2022). Only the fibula is sigmoid and anteriorly projected, but lateromedially narrow with an expanded anteromedially crest, which is larger anteroposteriorly than in *Lohuecotitan*, *Lirainosaurus* (Vila et al., 2022) and probably like those of *Magyarosaurus*, and is the single character that resembles our PC1 results.

Moreover, we must consider that our age estimations for the nodes of our supertree are extremely conservative and are based on the topology after the reduced tips of our sample (see Table 1). Titanosaurian sauropods appeared unambiguously during the Early Cretaceous (D'Emic, 2012; Mannion et al., 2019b; Poropat et al., 2016) just as lithostrotian titanosaurs appeared early after the Valanginian-Hauterivian (Mannion et al., 2019b; Poropat et al., 2016). Considering several recent phylogenetic hypotheses, the colossosaurian node may have branched in the early Albian (Gorscak et al., 2023; Sallam et al., 2018; Vila et al., 2022). Saltasauridae have also often been estimated at the transit between the Early Cretaceous and Late Cretaceous, with *Jiangshanosaurus* considered an early-branching saltasaurid (Poropat et al., 2016). However, the recent redescription of *Jiangshanosaurus* material has shed light on its phylogenetic affinities and it may be an euhelopodid or at least not as a deeply branched titanosaur (Mannion et al., 2019a). Saltasaurid lithostrotians are nevertheless traced back to the late Albian in recent studies (Sallam et al. 2018; Vila et al., 2022). The trends observed in our study may be accentuated with still a general body size decrease among lithostrotian sauropods (Fig 9a). However, a series of convergences in the appendicular skeleton: e.g., the acquisition of

the plesiomorphic columnar titanosaur hind limb among medium to large lithostrotians, seem to evolve independently of body size (e.g., Fig. 7b). Recent phylogenetic hypotheses show uncertain phylogenetic affinities for some of the sauropods studied, particularly for some of the lithostrotian taxa. This is the case of the Opisthocoelicaudiinae affinities that have been suggested for some members of Lirainosaurinae and *Lohuecotitan*, which is also proposed as a subclade within Saltasauridae (Vila et al., 2022) as Opisthocoelicaudiinae. *Atsinganosaurus* an Ibero-Armorican lithostrotian was recently recovered as member of Lirainosaurinae (Díez Díaz et al., 2020, 2018) or as a lognkosaurian colossosaur (Gorscak and O'Connor, 2019; Vila et al., 2022). *Atsinganosaurus* is a small lithostrotian with a hind limb morphology similar to that of *Lirainosaurus* (Díez Díaz et al., 2018). The extremely gracile limbs of *Atsinganosaurus* resemble those of the small rinconsaurian lithostrotians (González Riga et al., 2019; this study) or even the large *Mendozasaurus*. However, its affinities to Colossosauria will still indicate a convergence between small Opisthocoelicaudiinae and lognkosaurian colossosaurs according to the phylogenetic hypothesis of Vila et al. (2022). This phylogenetic hypothesis still indicates that the large-sized titanosaurs like *Dreadnoughtus* and *Alamosaurus* (robust medially bevelled femur and sigmoid fibula; see Lehman and Coulson, 2002; Wick and Lehman, 2014) exhibit a morphologically convergence in the hind limb with the small saltasaurines like *Neuquensaurus* and *Saltasaurus*.

It seems that these morphological similarities are due to other biomechanical aspects after the acquisition of the arched hind limb within Somphospondyli, as well as to other morphological features related to the wide-gauge posture of the appendicular skeleton. It is possible that minor differences that do not show a significant phylogenetic signal and recover in other shape-PCs (Appendix S4), are key features for other adaptations that are also important such as the trade-off between speed and rearing stability, which may have shaped limb morphology in the Titanosauriformes, particularly in the zeugopods (e.g., Upchurch et al., 2021).

3.3. Caveats of this study

Our analyses include a wide range of titanosaurs from most of the proposed subclades. However, many hind limb elements are fragmentary and required virtual restoration according to Páramo et al. (2020, 2022). Traditional studies propose excluding incomplete specimens from the sample. However, in this case, several of our taxa from an already small sample (n = 17) could not be included in this study because they do not have complete specimens to calculate the mean shape for each hind limb element type (e.g., *Mendozasaurus neguyelap* with several tibia and fibula specimens, *Oceanotitan dantasi* with only the fragmentary elements of its left hind limb). The exclusion of potentially informative areas or taxa may hinder palaeobiological studies (Brown et al., 2012) and landmarks estimation may be a more informative procedure (Arbour and Brown, 2014; Brown et al., 2012). Also, it may be interesting to include several taxa that have been examined in previous studies (e.g., Páramo et al., 2020), but many of these taxa lack one or more hind limb element types. In this case, we did not choose to estimate the entire morphology of an element type, because we lack the necessary and more powerful tools to do so, such as partial least squares estimation methods (e.g., Torres-Tamayo *et al.* 2020).

Our reconstructions of the analyzed titanosaurian hind limbs can also bias our study. The lack of the astragalus in most of the titanosaurs studied (whether due to the lack of available 3D-scanned specimens or the lack of a preserved astragalus) hinders the estimation of the position of the zeugopodial elements. This study uses the most conservative assumption in the overall position of the distal part of the hind limb as the fibula could be positioned even more distally, without reaching proximally the femur, and interlocked with the tibia in several specimens (e.g., *Neuquensaurus australis*, specimen MCS-5-25/26, APB. pers. obs.). This is especially relevant

for the robust and arched hind limb with extremely robust zeugopodia, as *Dreadnoughtus schrani*, *Neuquensaurus* spp., and *Saltasaurus loricatus*, but see also *Uberabatitan riberoi* (Salgado and Carvalho, 2008).

The sample is also small and we did not opt to include several advanced statistical hypothesis tests like phylogenetic convergence (Stayton, 2015) because it did not meet the requirements. Instead, we chose a conservative set of tests to discuss the true morphological convergence over titanosaurian hind limb evolution with a mix of phylogenetic and non-phylogenetic methods. We chose Butler & Gowsami (2008) change frequencies analysis because, although its statistical properties are less well known than those of independent contrast analyses, it is less sensitive to topological imprecision and somewhat independent of branch length differences (Butler and Goswami, 2008; de Souza and Santucci, 2014). Following this reasoning, we also decided not to estimate independent phylogenetic contrasts that may be sensitive to large differences in branch length in our lithostrotian-biased sample to test for trait correlation between shape-PCs against log-transformed centroid size, contrary to previous studies (Bates et al., 2016). Instead, we opted for the traditional use of test for correlation between tree tips (specimens) shape-PCs against log-transformed centroid sizes via RMA and without incorporating the phylogenetic tree topology of our current time-calibrated supertree.

4. Conclusions

Our results suggest that the main features related to the acquisition of an arched hind limb posture (presence of lateromedially wide femora with robust zeugopods) are typical of more deeply nested titanosaurs such as saltasaurines (Carrano, 2005; Lefebvre et al., 2022; Sander et al., 2011; Ullmann et al., 2017; Vila et al., 2022; Wilson and Carrano, 1999) and exhibit a significant phylogenetic signal about titanosaurian evolution (Table 5, Fig. 7). The arched morphology usually related with wide-gauge posture is an exaptation initially related to increasing body size. However, once fully acquired within Somphospondyli, these features are no longer related to increasing body size, as increases in the arched posture and the development of hyper-robust zeugopods are features that evolved independently in several lineages, and are shared by several of both the smallest and largest taxa in different titanosaurian lineages (Fig. 6, Table 4). Also, there is an evolutionary trend toward decreasing titanosaurian hind limb size (and body size; Fig. 7), based on the size of the hind limb centroid. This trend is congruent with previous studies focused on the size evolution within Titanosauriformes (de Souza and Santucci 2014), despite an increase in arched morphology and robustness of the hind limb in deeply nested titanosaurian subclades.

The lack of correlation between the arched posture, position and robustness of zeugopod, among other traits with the body size may also be related to a wide morphological variation within Lithostrotia (Figs. 2-4). It can be noted that, together with a trend toward increasingly arched hind limbs and reduced zeugopods with increasingly rotated fibulae, there is also a large morphological convergence between the different titanosaurian subclades, as indicated by both our non-phylogenetic and phylogenetic analyses (Table 2-3). Many of the morphological changes without a significant signal in titanosaurian evolution are related to the morphology and anatomical position of zeugopod bones. Large morphological convergences unrelated to body size may be a response to different morphofunctional adaptations. Our results show several differences in the morphology of zeugopod elements without a signal in the evolution of titanosaurs, especially those regarding the fibula (rotation, sigmoidal morphology, anterior or posterior displacement of the proximal end that affects the anteroposterior position of the lateral bulge). These morphological differences are also related to its relative position and articulation with the tibia and correlate with the expression of femoral features like the relative development

of the posterior epicondyle of the fibular condyle. These features translate in changes in the length and morphology of the hind limb distal musculature that exhibit no clear evolutionary trend within titanosaurs, as previous studies have indicated. Also, our results show that specimens in different subclades share similar morphologies across the shape-PCs that exhibit no phylogenetical signal in titanosaurian evolution. The observed changes in the zeugopod morphology may be related to different morphofunctional and ecomorphological adaptations and the convergences in hind limb morphology of titanosaurs may explain biomechanical similarities. This may explain the differences observed between small and medium-to-large titanosaurs with either arched or columnar hind limbs (i.e. PC1 similarities) across those shape-PCs that lack a significant signal in the evolution of titanosaurs. However, to test the hypothesis of differences in biomechanical adaptation (i.e., movement speed or differences in feeding niche specialization) further analyses with additional parts of the skeleton must be included.

5. Acknowledgments

This work is funded by Ministry of Science and Innovation of Spain project PID2019-111488RB-I00 and the Junta de Comunidades de Castilla-La Mancha projects (SBPLY/19/180801/000044 and SBPLY/21/180801/000045). Access to fossil vertebrate collections in Argentina was made possible by Spanish Ministry of Economy and Competitiveness grant EEBB-I-16-11875. The authors would like to thank BP. Kear and Uppsala University Natural History Museum staff for facilitating access to their collections. Access to Uppsala University Museum of Natural History paleovertebrate collections was possible thanks to the ERG-2020 EAVP research grant. Digitizing of macronarian sauropod *Oceanotitan dantasi* holotype was enabled by the ERG-2020 EAVP research grant. Author PM was funded by FCT/MCTES for one CEEC Individual contract (CEECIND/00726/2017) and a Haaga Family Postdoctoral Fellow (2016-2018) in the NHMLA (CA, USA). The authors are very grateful to S. Chapman and Natural History Museum of London (UK) staff for facilitating access to their collections. Access to NHM (UK) was made possible thanks to the European Union Council Synthesys program GB-TAF-6153. They also want to thank the students of the Faculty of Arts in the UCM (Madrid, Spain) and preparation staff for providing the sample for this study. They equally thank many others for access to specimens under their care, including S. Langreo at the Museo de Paleontología de Castilla-La Mancha (Cuenca, Spain); J.A. Ramírez de la Peciña and C. Corral at the MCNA (Vitoria, Spain); R. Coria at the MCF (Plaza Huincul, Argentina); L. Filippi at the MRS (Rincón de los Sauces, Argentina); M. Reguero at the MLP (La Plata, Argentina); A. Otero at CONICET (La Plata, Argentina); S. Devincenzi at the IANIGLA (Mendoza, Argentina); and B. González Riga at the UNCUYO (Mendoza, Argentina); C. Muñoz at the MPCA (Cipolletti, Argentina); I. Cerda fromat the CONICET (Cipolletti, Argentina); P. Ortiz at the PVL (Tucumán, Argentina); A.G. Kramarz and M. Ezcurra at the MACN (Buenos Aires, Argentina) and J. Le Loeuff at the Musée des Dinosauries d'Espéraza (Espéraza, France). We want to ask M Christopher for access to *D. schrani* skeleton 3D scan. We want to thank P.M. Sander for his comments which helped improve this manuscript.

6. Bibliography

Arbour JH, Brown CM. 2014. Incomplete specimens in geometric morphometric analyses. *Methods in Ecology and Evoution* **5**:16–26. doi:10.1111/2041-210X.12128

Bates KT, Mannion PD, Falkingham PL, Brusatte SL, Hutchinson JR, Otero A, Sellers WI, Sullivan C, Stevens KA, Allen V. 2016. Temporal and phylogenetic evolution of the

sauropod dinosaur body plan. *Royal Society Open Science* **3**:150636. doi:10.1098/rsos.150636

Bininda-Emonds ORP. 2004. The evolution of supertrees. *Trends in ecology & evolution* **19**:315–22. doi:10.1016/j.tree.2004.03.015

Bonaparte JF, Coria RA. 1993. Un nuevo y gigantesco saurópodo Titanosaurio de la Formación Río Limay (Albiano-Cenomaniano) de la provincia del Neuquén, Argentina. *Ameghiniana* **30**:271–282.

Bonnan MF. 2007. Linear and geometric morphometric analysis of long bone scaling patterns in Jurassic Neosauropod Dinosaurs: Their Functional and Paleobiological Implications. *The Anatomical Record: Advances in Integrative Anatomy and Evolutionary Biology* **290**:1089–1111. doi:10.1002/ar.20578

Bonnan MF, Wilhite RD, Masters SL, Yates AM, Gardner CK, Aguiar A. 2013. What lies beneath: sub-articular long bone shape scaling in eutherian mammals and saurischian dinosaurs suggests different locomotor adaptations for gigantism. *PLOS ONE* **8**:e75216. doi:10.1371/journal.pone.0075216

Borsuk-Bialynicka M. 1977. A new camarasaurid sauropod *Opisthocoelicaudia skarzynskii* gen. n., sp. n. from the Upper Cretaceous of Mongolia. *Paleontologia Polonica* **37**:5–64.

Brown CM, Arbour JH, Jackson DA. 2012. Testing of the effect of missing data estimation and distribution in morphometric multivariate data analyses. *Systematic Biology* **61**:941–954. doi:10.1093/sysbio/sys047

Butler RJ, Goswami A. 2008. Body size evolution in Mesozoic birds: little evidence for Cope's rule. *Journal of Evolutionary Biology* **21**:1673–1682. doi:10.1111/j.1420-9101.2008.01594.x

Carballido JL, Pol D, Otero A, Cerda IA, Salgado JL, Garrido AC, Ramezani J, Cúneo NR, Krause JM. 2017. A new giant titanosaur sheds light on body mass evolution among sauropod dinosaurs. *Proceedings of the Royal Society B: Biological Sciences* **284**:20171219. doi:10.1098/rspb.2017.1219

Carrano MT. 2006. Body-Size Evolution in the Dinosauria In: Carrano MT, Gaudin TJ, Blob RW, Wible J, editors. Amniote Paleobiology: Perspectives on the Evolution of Mammals, Birds, and Reptiles. Chicago University Press. pp. 225–268.

Carrano MT. 2005. The evolution of sauropod locomotion In: Curry Rogers KA, Wilson JA, editors. The Sauropods: Evolution and Paleobiology. University of California Press. pp. 229–250.

Curry Rogers K. 2009. The postcranial osteology of *Rapetosaurus krausei* (Sauropoda: Titanosauria) from the Late Cretaceous of Madagascar. *Journal of Vertebrate Paleontology* **29**:1046–1086. doi:10.1671/039.029.0432

de Souza LM, Santucci RM. 2014. Body size evolution in Titanosauriformes (Sauropoda, Macronaria). *Journal of Evolutionary Biology* **27**:2001–2012. doi:10.1111/jeb.12456

D'Emic MD. 2012. The early evolution of titanosauriform sauropod dinosaurs. *Zoological Journal of the Linnean Society* **166**:624–671. doi:10.1111/j.1096-3642.2012.00853.x

Díez Díaz V, Garcia G, Pereda Suberbiola X, Jentgen-Ceschino B, Stein K, Godefroit P, Valentin X. 2020. A new titanosaur (Dinosauria: Sauropoda) from the Upper Cretaceous of Velaux-La-Bastide Neuve (southern France). *Historical Biology* **00**:1–20. doi:10.1080/08912963.2020.1841184

Díez Díaz V, Garcia G, Pereda-Suberbiola X, Jentgen-Ceschino B, Stein K, Godefroit P, Valentin X. 2018. The titanosaurian dinosaur *Atsinganosaurus velauciensis* (Sauropoda) from the Upper Cretaceous of southern France: New material, phylogenetic affinities, and palaeobiogeographical implications. *Cretaceous Research* **91**:429–456. doi:10.1016/j.cretres.2018.06.015

González Riga BJ, Lammana MC, Otero A, Leonardo D. Ortiz D, Kellner AW, Ibiricu LM. 2019. An overview of the appendicular skeletal anatomy of South American titanosaurian sauropods, with definition of a newly recognized clade. *Anais da Academia Brasileira de Ciências* **91**:e20180374. doi:https://doi.org/10.1590/0001-3765201920180374

González Riga BJ, Mannion PD, Poropat SF, Ortiz David LD, Coria JP. 2018. Osteology of the Late Cretaceous Argentinean sauropod dinosaur *Mendozasaurus neguyelap*: implications for basal titanosaur relationships. *Zoological Journal of the Linnean Society* 1–46. doi:10.1093/zoolinnean/zlx103/4816851

Gorscak E, Lamanna M, Schwarz D, Díez Díaz V, Salem B, Sallam H, Wiechmann M. 2023. A new titanosaurian (Dinosauria: Sauropoda) from the Upper Cretaceous (Campanian) Quseir Formation of the Kharga Oasis, Egypt. *Journal of Vertebrate Paleontology*. doi:10.1080/02724634.2023.2199810

Gorscak E, O'Connor PM. 2019. A new African Titanosaurian Sauropod Dinosaur from the middle Cretaceous Galula Formation (Mtuka Member), Rukwa Rift Basin, Southwestern Tanzania. *PLOS ONE* **14**:e0211412. doi:10.1371/journal.pone.0211412

Gunz P, Mitteroecker P, Bookstein FL. 2005. Semilandmarks in three dimensions In: Slice DE, editor. Modern Morphometrics in Physical Anthropology. Springer. pp. 73–98.

Henderson DM. 2006. Burly gaits: Centers of mass, stability, and the trackways of sauropod dinosaurs. *Journal of Vertebrate Paleontology* **26**:907–921. doi:10.1671/0272-4634(2006)26

Holliday CM, Ridgely RC, Sedlmayr JC, Witmer LM. 2010. Cartilaginous epiphyses in extant archosaurs and their implications for reconstructing limb function in dinosaurs. *PloS one* **5**:1–16. doi:10.1371/journal.pone.0013120

Klinkhamer AJ, Mallison H, Poropat SF, Sloan T, Wroe S. 2019. Comparative three-dimensional moment arm analysis of the sauropod forelimb: implications for the transition to a wide-gauge stance in titanosaurs. *The Anatomical Record* **302**:794–817. doi:10.1002/ar.23977

Lacovara KJ, Lamanna MC, Ibiricu LM, Poole JC, Schroeter ER, Ullmann PV, Voegele KK, Boles ZM, Carter AM, Fowler EK, Egerton VM, Moyer AE, Coughenour CL, Schein JP, Harris JD, Martínez RD, Novas FE. 2014. A gigantic, exceptionally complete titanosaurian sauropod dinosaur from Southern Patagonia, Argentina. *Scientific Reports* **4**. doi:10.1038/srep06196

Lefebvre R, Houssaye A, Mallison H, Cornette R, Allain R. 2022. A path to gigantism: Three□dimensional study of the sauropodomorph limb long bone shape variation in the context of the emergence of the sauropod bauplan. *Journal of Anatomy*. doi:10.1111/joa.13646

Legendre P. 2018. lmodel2: Model II Regression. R package version 1.7-3, https://CRAN.R-project.org/package=lmodel2

Lehman TM, Coulson AB. 2002. A juvenile specimen of the sauropod dinosaur alamosaurus sanjuanensis from the Upper Cretaceous of Big Bend National Park, Texas. *Journal of Paleontology* **76**:156–172. doi:10.1666/0022-3360(2002)076<0156:AJSOTS>2.0.CO;2

Lu JC, Xu L, Jia SH, Zhang XL, Zhang JM, Yang LL, You HL, Ji Q. 2009. A new gigantic sauropod dinosaur from the Cretaceous of Ruyang, Henan, China. *Geological Bulletin of China* **28**:1–10. doi:10.1111/j.1095-8312.1965.tb00944.x

Mallison H. 2011. Digitizing methods for paleontology: Applications, benefits and limitations In: Elewa A, editor. Computational Paleontology. Springer. pp. 7–43.

Mannion PD, Upchurch P. 2010. A quantitative analysis of environmental associations in sauropod dinosaurs. *Paleobiology* **36**:253–282. doi:10.1666/08085.1

Mannion PD, Upchurch P, Jin X, Zheng W. 2019a. New information on the Cretaceous sauropod dinosaurs of Zhejiang Province, China: Impact on Laurasian titanosauriform phylogeny and biogeography. *Royal Society Open Science* **6**. doi:10.1098/rsos.191057

Mannion PD, Upchurch P, Schwarz D, Wings O. 2019b. Taxonomic affinities of the putative titanosaurs from the Late Jurassic Tendaguru Formation of Tanzania: phylogenetic and biogeographic implications for eusauropod dinosaur evolution. *Zoological Journal of the Linnean Society* **185**:784–909. doi:10.1093/zoolinnean/zly068

Mazzetta GV, Christiansen P, Fariña R a. 2004. Giants and bizarres: body size of some southern south american cretaceous dinosaurs. *Historical Biology* **16**:71–83. doi:10.1080/08912960410001715132

Mocho P, Royo-Torres R, Ortega F. 2019. A new macronarian sauropod from the Upper Jurassic of Portugal. *Journal of Vertebrate Paleontology* **39**:1–23. doi:10.1080/02724634.2019.1578782

Navarro BA, Ghilardi AM, Aureliano T, Díaz VD, Bandeira KLN, Cattaruzzi AGS, Iori FV, Martine AM, Carvalho AB, Anelli LE, Fernandes MA, Zaher H. 2022. A new nanoid titanosaur (Dinosauria, Sauropoda) from the Upper Cretaceous of Brazil. *Ameghiniana* **59**:317–354. doi:10.5710/AMGH.25.08.2022.3477

Otero A, Carballido JL, Moreno AP. 2020. The appendicular osteology of *Patagotitan Mayorum* (Dinosauria, Sauropoda). *Journal of Vertebrate Paleontology* **40**:1–19. doi:10.1080/02724634.2020.1793158

Páramo A, Mocho P, Ortega F. 2020. Three-dimensional analysis of the titanosaurian limb skeleton: implications for systematic analysis. *Journal of Iberian Geology* **46**:369–402. doi:10.1007/s41513-020-00139-8

Poropat SF, Kundrát M, Mannion PD, Upchurch P, Tischler TR, Elliott DA. 2021. Second specimen of the Late Cretaceous Australian sauropod dinosaur *Diamantinasaurus matildae* provides new anatomical information on the skull and neck of early titanosaurs. *Zoological Journal of the Linnean Society* **192**:610–674. doi:10.1093/zoolinnean/zlaa173

Poropat SF, Mannion PD, Upchurch P, Hocknull SA, Kear BP, Kundrát M, Tischler TR, Sloan T, Sinapius GHK, Elliott JA, Elliott DA. 2016. New Australian sauropods shed light on Cretaceous dinosaur palaeobiogeography. *Scientific Reports* **6**:1–12. doi:10.1038/srep34467

Poropat SF, Upchurch P, Mannion PD, Hocknull SA, Kear BP, Sloan T, Sinapius GHK, Elliott DA. 2015. Revision of the sauropod dinosaur *Diamantinasaurus matildae* Hocknull et al. 2009 from the mid-Cretaceous of Australia: Implications for Gondwanan titanosauriform dispersal. *Gondwana Research* **27**:995–1033. doi:10.1016/j.gr.2014.03.014

R Core Team. 2022. R: A Language and Environment for Statistical Computing. Vienna, Austria: R Foundation for Statistical Computing.

Revell LJ. 2012. phytools: An R package for phylogenetic comparative biology (and other things). *Methods in Ecology and Evolution* **3**:217–223.

Royo-Torres R. 2009. El saurópodo de Peñarroya de Tastavins. *Monograpfías Turonlenses* **6**:1–548.

Salgado JL, Carvalho IDS. 2008. *Uberabatitan ribeiroi*, a new titanosaur from the Marília Formation (Bauru Group, Upper Cretaceous), Minas Gerais, Brazil. *Palaeontology* **51**:881–901. doi:10.1111/j.1475-4983.2008.00781.x

Salgado L, Coria RA, Calvo JO. 1997. Evolution of titanosaurid sauropods: Phytogenetic analysis based on the postcranial evidence. *Ameghiniana* **34**:3–32.

Sallam HM, Gorscak E, O'Connor PM, El-Dawoudi IA, El-Sayed S, Saber S, Kora MA, Sertich JJW, Seiffert ER, Lamanna MC. 2018. New Egyptian sauropod reveals Late Cretaceous dinosaur dispersal between Europe and Africa. *Nature Ecology & Evolution* **2**:445–451. doi:10.1038/s41559-017-0455-5

Sander PM. 2013. An Evolutionary Cascade Model for Sauropod Dinosaur Gigantism - Overview, Update and Tests. *PLOS ONE* **8**:e78573. doi:10.1371/journal.pone.0078573

Sander PM, Christian A, Clauss M, Fechner R, Gee CT, Griebeler E-M, Gunga H-C, Hummel J, Mallison H, Perry SF, Preuschoft H, Rauhut OWM, Remes K, Tütken T, Wings O, Witzel U. 2011. Biology of the sauropod dinosaurs: the evolution of gigantism. *Biological Reviews* **86**:117–155. doi:10.1111/j.1469-185X.2010.00137.x

Schlager S. 2017. Morpho and Rvcg – Shape Analysis in R In: Zheng G, Li S, Szekely G, editors. Statistical Shape and Deformation Analysis. Elsevier. pp. 217–256. doi:10.1016/B978-0-12-810493-4.00011-0

Schliep K, Potts AJ, Morrison DA, Grimm GW. 2017. Intertwining phylogenetic trees and networks. *Methods in Ecology and Evolution* **8**:1212–1220.

Schliep KP. 2011. phangorn: phylogenetic analysis in R. *Bioinformatics* **27**:592–593. doi:10.1093/bioinformatics/btq706

Schwarz D, Wings O, Meyer CA. 2007. Super sizing the giants: first cartilage preservation at a sauropod dinosaur limb joint. *Journal of the Geological Society* **164**:61–65. doi:10.1144/0016-76492006-019

Silva Junior JCG, Martinelli AG, Iori FV, Marinho TS, Hechenleitner EM, Langer MC. 2022. Reassessment of Aeolosaurus maximus, a titanosaur dinosaur from the Late Cretaceous of Southeastern Brazil. *Historical Biology* **34**:403–411. doi:10.1080/08912963.2021.1920016

Stayton C. 2015. The definition, recognition, and interpretation of convergent evolution, and two new measures for quantifying and assessing the significance of convergence. *Evolution* **69**. doi:10.1111/evo.12729

Torres-Tamayo N, Schlager S, García-Martínez D, Sanchis-Gimeno JA, Nalla S, Ogihara N, Oishi M, Martelli S, Bastir M. 2020. Three-dimensional geometric morphometrics of thorax-pelvis covariation and its potential for predicting the thorax morphology: A case study on Kebara 2 Neandertal. *Journal of Human Evolution* **147**:102854. doi:10.1016/j.jhevol.2020.102854

Ullmann PV, Bonnan MF, Lacovara KJ. 2017. Characterizing the evolution of wide-gauge features in stylopodial limb elements of titanosauriform sauropods via geometric morphometrics. *The Anatomical Record* **300**:1618–1635. doi:10.1002/ar.23607

Ullmann PV, Lacovara KJ. 2016. Appendicular osteology of *Dreadnoughtus schrani*, a giant titanosaurian (Sauropoda, Titanosauria) from the Upper Cretaceous of Patagonia, Argentina. *Journal of Vertebrate Paleontology* **36**. doi:10.1080/02724634.2016.1225303

Upchurch P, Barrett PM, Dodson P. 2004. Sauropoda In: Weishampel DB, Dodson P, Osmolska H, editors. The Dinosauria. Berkeley and Los Angeles: University of California Press. pp. 259–322.

Upchurch P, Mannion PD, Xu X, Barrett PM. 2021. Re-assessment of the Late Jurassic eusauropod dinosaur *Hudiesaurus sinojapanorum* Dong, 1997, from the Turpan Basin, China, and the evolution of hyper-robust antebrachia in sauropods. *Journal of Vertebrate Paleontology* **41**. doi:10.1080/02724634.2021.1994414

Vidal D, Mocho P, Aberasturi A, Sanz JL, Ortega F. 2020. High browsing skeletal adaptations in *Spinophorosaurus* reveal an evolutionary innovation in sauropod dinosaurs. *Scientific Reports* **10**:1–10. doi:10.1038/s41598-020-63439-0

Vila B, Sellés A, Moreno-Azanza M, Razzolini NL, Gil-Delgado A, Canudo JI, Galobart À. 2022. A titanosaurian sauropod with Gondwanan affinities in the latest Cretaceous of Europe. *Nature Ecology & Evolution*. doi:10.1038/s41559-021-01651-5

Voegele KK, Bonnan MF, Siegler S, Langel CR, Lacovara KJ. 2022. Constraining morphologies of soft tissues in extinct vertebrates using multibody dynamic simulations: a case study on articular cartilage of the sauropod *Dreadnoughtus*. *Frontiers in Earth Science* **10**. doi:10.3389/feart.2022.786247

Voegele KK, Ullmann PV, Lamanna MC, Lacovara KJ. 2021. Myological reconstruction of the pelvic girdle and hind limb of the giant titanosaurian sauropod dinosaur *Dreadnoughtus schrani*. *Journal of Anatomy* **238**:576–597. doi:10.1111/joa.13334

Voegele KK, Ullmann PV, Lamanna MC, Lacovara KJ. 2020. Appendicular myological reconstruction of the forelimb of the giant titanosaurian sauropod dinosaur *Dreadnoughtus schrani*. *Journal of Anatomy* 1–22. doi:10.1111/joa.13176

Wick SL, Lehman TM. 2014. A complete titanosaur femur from West Texas with comments regarding hindlimb posture. *Cretaceous Research* **49**:39–44. doi:10.1016/j.cretres.2014.02.003

Wiley DF, Amenta N, Alcantara DA, Ghosh D, Kil YJ, Delson E, Harcourt-Smith W, Rohlf FJ, St John K, Hamann B. 2005. Evolutionary morphing. IEEE Visualization, 2005. VIS 05. pp. 431–438. doi:10.1109/VISUAL.2005.1532826

Wilson JA, Carrano MT. 1999. Titanosaurs and the origin of “wide-gauge” trackways; a biomechanical and systematic perspective on sauropod locomotion. *Paleobiology* **25**:252–267.

Wilson JeffreyA. 2002. Sauropod dinosaur phylogeny: critique and cladistic analysis. *Zoological Journal of the Linnean Society* **136**:215–275. doi:10.1046/j.1096-3642.2002.00029.x

Zurriaguz VL, Cerda IA. 2017. Caudal pneumaticity in derived titanosaurs (Dinosauria: Sauropoda). *Cretaceous Research* **73**:14–24. doi:10.1016/j.cretres.2017.01.001

7. Methods

7.1. 3D Geometric Morphometrics

To analyse the morphology, 17 macronarian sauropod hind limbs (Table 1) were 3D-digitized and anayzed using 3D Geometric Morphometrics tool-kit (3D-GMM; Gunz et al., 2005 e.g., Páramo et al., 2020). The 3D digitizing process was based on the methodology proposed in previous analyses (i.e., Mallison, 2011; Páramo et al., 2020) and 3D-GMM analyses were conducted in R statistical software v4.1.3 (R Core Team, 2022).

To reconstruct each taxa hind limb, we first virtually-restored the 3D reconstructions of the digitized femora, tibiae and fibulae and calculated the grand mean shape for each sampled taxon using previous datasets (Páramo et al., 2020). The grand mean specimens for each taxon were mounted on an estimated anatomical position (accounting for the lack of astragalus in our sample to guide the distal zeugopod articulation). A comprehensive description of the methodology can be accessed in Appendix 2.

Each element of the hind limb is separated by an articular cap much larger than in other known extant archosaurs (Bonnan et al., 2013; Holliday et al., 2010; Schwarz et al., 2007; Voegele et al., 2022). The femur, and the hind limb overall, may exhibit the best correlation between cartilage cap and bone morphology constrained by its role as support under most of the stress of the body mass (Bonnan et,al., 2013; Voegele et al., 2022). Although cartilaginous cap thickness is not constant and may vary among taxa, we set up our model hind limbs with a similar constant space between the femur and the zeugopod bones in all the sampled taxa. The anatomical mounts include an additional space of 2% of the element length between stylopod and zeugopod (following Voegele et al., 2022).

A total of 28 landmarks and 12 semilandmark curves were placed on the hind limb bones partly based on previous studies (Lefebvre et al., 2022; Páramo et al., 2020; Table 2, Fig. 2, Appendix 1) using IDAV Landmark Editor software (Wiley et al., 2005) (dataset with the landmark and semilandmark curves coordinates can be accessed in the Appendix S1. Semilandmarks were then slid in R using package “Morpho” (Schlager, 2017) following Gunz et al., (2005). To remove size differences, spatial position and orientation, the resulting landmark and semilandmark configurations were superimposed via Generalized Procrustes Analysis (GPA) using the “procSym” function in *Morpho* package. Morphological variance was analysed with Principal Component Analysis (PCA; results in Table 3), saving the expected number of Principal Components (PCs) which summarize a significant amount of variance after an Anderson Chi’s test (see Bonnan, 2007).

Evolutionary trend analyses were accomplished after the estimation of a consensus tree topology using the MRP-supertree methodology (Bininda-Emonds, 2004) with the *phangorn* package (Schliep et al., 2017; Schliep, 2011). For supertree construction we compiled several of the more recent phylogenetic hypotheses that include all the available sampled data (resulting supertree can be accessed in Appendix 1; trimmed supertree in Fig. 2). The resulting phylogenetic relationships were projected onto the shape-PCA to visualize the phylomorphospace. To analyse true morphological convergences between titanosaurian sub-

clades, we tested for morphological differences in the hind limb skeleton using the shape variables (PCs) without the phylogenetic relationships involved using: (i) Mann Whitney U's test and Kruskal-Wallis non-parametric tests accounting for the uneven distribution of the group (sub-clade) samples and (ii) phylogenetic ANOVA using the time-calibrated supertree topology with the *phytools* R package (Revell, 2012).

7.2. Hind limb size distribution and phylogenetic signal

Sauropod body mass was proxied by hind limb centroid size collected from the GPA. Body mass can be calculated preferably using both humeral and femoral measurements (Mazzetta et al., 2004) or a whole-body volumetric estimation (Bates et al., 2016). However, as the hind limb is the main sauropod body mass support, it can be better used as a "conservative-minimal" approach to its body mass, with larger hind limb corresponding to giant titanosaurian taxa. We tested for allometric relationships between the sauropod hind limb shape variables (PCs) and the centroid size as proxy to body mass via Reduced Major Axis (RMA) regression using *lmodel2* R package (Legendre, 2018)(Legendre 2018).

We used the time-calibrated supertree topology and our shape variables (PCs) and hind limb centroid size to generate the Pagel's lambda (λ) with the "phytools" R package and test for the phylogenetic signal of these traits. All hypotheses of statistical correlations, dissimilarity tests and phylogenetic signal tests were accepted as significant using an alpha level of 0.05 (a comprehensive report of the results and a copy of the R code and packages used can be accessed in Appendix S4 and S5 respectively). Once those PCs that exhibit significant phylogenetical signal were identified, as well as the log-transformed centroid size, we estimated their ancestral characters (ACEs) using maximum-likelihood and a simple Brownian evolutionary model similar to the one assumed for estimation of the Pagel's lambda. We used the ACEs to observe trends in the evolution of titanosaurian hind limb size and morphology (based on our shape-PCs). We evaluated the differences in body size (proxied by log-transformed hind limb centroid size ACEs) between terminal taxa and internal nodes and between internal nodes of Titanosauriformes, Somphospondyli, Titanosauria and Lithostrotia, as well as their subclades. The sum of changes, mean change, median change, positive, negative and the total amount of changes were evaluated for each of the above clades following Butler and Goswami (2008). We used a $\chi 2$ goodness-of-fit test to evaluate whether body size increasing or decreasing, and shape-PCs occur at the same frequency (50%-50% null hypothesis) or have a positive or negative tendency over titanosaurian evolution.

FIGURE CAPTIONS

Figure 1. Sample of several 3D reconstruction of macronarian hind limbs used in this study. (a) *Oceanotitan dantasi*; (b) *Ligabuesarusu leanzai*; (c) *Lohuecotitan pandafilandi*; (d) *Saltasaurus loricatus*. All taxa in anterior and posterior views.

Figure 2. PCA results on the GPA aligned landmark and semilandmark curves of the hind limb. (a) PC1-PC2 biplot. (b) PC1-PC2 phylomorphospace with projected phylogenetic tree. (c) Representation of the shape change along PC1, blue are negative scores, red are positive scores. Percentage of variance of each PC in brackets under corresponding axis. *Ae – Aeolosaurus*, *Amp – Ampelosaurus*, *An – Antarctosaurus*, *Bo – Bonatitan*, *Bon – Bonitasaura*, *Dre – Dreadnoughuts*, *Eu – Euhelopus*, *Ja – Jainosaurus*, *Li – Lirainosaurus*, *Lig – Ligabuesaurus*,

Lo – Lohuecotitan, Ma – Magyarosaurus, Me – Mendozasaurus, Mu – Muyelensaurus, Ne – Neuquensaurus, Sa – Saltasaurus.

Figure 3. PCA results for the GPA aligned landmark and semilandmark curves of the hind limbs. (a) PC2-PC3 biplot. (b) PC2-PC3 phylomorphospace with projected phylogenetic tree. (c) Representation of the shape change along PC2, blue are negative scores, red are positive scores. Percentage of variance of each PC in brackets under corresponding axis. *Ae – Aeolosaurus, Amp – Ampelosaurus, An – Antarctosaurus, Bo – Bonatitan, Bon – Bonitasaura, Dre – Dreadnoughuts, Eu – Euhelopus, Ja – Jainosaurus, Li – Lirainosaurus, Lig – Ligabuesaurus, Lo – Lohuecotitan, Ma – Magyarosaurus, Me – Mendozasaurus, Mu – Muyelensaurus, Ne – Neuquensaurus, Sa – Saltasaurus.*

Figure 4. PCA results for the GPA aligned landmark and semilandmark curves of the hind limbs. (a) PC1-PC3 biplot. (b) PC1-PC3 phylomorphospace with projected phylogenetic tree. (c) Representation of the shape change along PC3, blue are negative scores, red are positive scores. Percentage of variance of each PC in brackets under corresponding axis. *Ae – Aeolosaurus, Amp – Ampelosaurus, An – Antarctosaurus, Bo – Bonatitan, Bon – Bonitasaura, Dre – Dreadnoughuts, Eu – Euhelopus, Ja – Jainosaurus, Li – Lirainosaurus, Lig – Ligabuesaurus, Lo – Lohuecotitan, Ma – Magyarosaurus, Me – Mendozasaurus, Mu – Muyelensaurus, Ne – Neuquensaurus, Sa – Saltasaurus.*

Figure 5. Time calibrated supertree with PC1-PC2 results and hind limb centroid size for each sauropod.

Figure 6. RMA results of the first three shape PCs against the logarithm of the hind limb centroid size. (a) PC1 against log-Centroid size, all taxa RMA in dark red: intercept = 0.221, slope = -0.102, r^2 = 0.105, p = 0.204; Titanosauria only partial RMA in dashed green: intercept = 0.203, slope = -0.092, r^2 = 0.118, p = 0.229; Lithostrotia only partial RMA in dotted orange: intercept = 0.246, slope = -0.120, r^2 = 0.319, p = 0.07; (b) PC2 against log-Centroid size, all taxa RMA in dark red: intercept = 0.155, slope = -0.072, r^2 = 0.054, p = 0.371; Titanosauria only partial RMA in dashed green: intercept = 0.158, slope = -0.075, r^2 = 0.117, p = 0.232; Lithostrotia only partial RMA in dotted orange: intercept = -0.127, slope = 0.066, r^2 = 0, p = 0.952; (c) PC3 against log-Centroid size (Csize), all taxa RMA in dark red: intercept = 0.137, slope = -0.064, r^2 = 0.055, p = 0.363; Titanosauria only partial RMA in dashed green: intercept = 0.110, slope = -0.055, r^2 = 0.236, p = 0.078; Lithostrotia only partial RMA in dotted orange: intercept = 0.140, slope = -0.073, r^2 = 0.313, p = 0.074. *Ae – Aeolosaurus, Amp – Ampelosaurus, An – Antarctosaurus, Bo – Bonatitan, Bon – Bonitasaura, Dre – Dreadnoughuts, Eu – Euhelopus, Ja – Jainosaurus, Li – Lirainosaurus, Lig – Ligabuesaurus, Lo – Lohuecotitan, Ma – Magyarosaurus, Me – Mendozasaurus, Mu – Muyelensaurus, Ne – Neuquensaurus, Sa – Saltasaurus.*

Figure 7. Evolution of log-transformed hind limb centroid size, shape PC1 and PC3 according to our sample and time-calibrated supertree topology. Ba – Barremian, Be – Berriasian, Ce – Cenomanian, Co – Conacian, H – Hauterivian, J – Jurassic, Late-K – Late Cretaceous, Ti –

Tithonian, Tu – Turonian, Va – Valanginian. my – million years from present, sc – subclade Colossosauria + *Bonitasaura*.

TABLE CAPTIONS

Table 1. Specimen sample used in this study. Proximodistal hind limb length measured in mm.

Table 2. PCA results over GPA aligned coordinates. Variance explained by each shape PC.

Table 3. Kruskal-Wallis test on shape PCA variables between the most inclusive subclades analysed.

Table 4. Phylogenetic ANOVA test on shape PCA variables between the most inclusive subclades studied.

Table 5. RMA models of the shape PCs against log-transformed Centroid size. CI – confidence interval.

Table 6. Estimated phylogenetic signal via Pagel's lambda. *p* value of log-likelihood ratio test after 1000 simulations. * Indicates significant relationships for an alpha of 0.05. log-Csize – Log-transformed hind limb centroid size.

Table 7. Results of pairwise ancestor-descendant comparisons for log-transformed centroid size in macronarian sauropods in our time-calibrated supertree (17 terminal taxa). n = ingroup internal nodes + terminal taxa. *= accepted as significant with alpha <0.05. º= Lithostrotia + *Antarctosaurus*.

Table 8. Results of ancestor-descendant pairwise comparisons for shape PC1 in macronarian sauropods in our time-calibrated supertree (17 terminal taxa). n = ingroup internal nodes + terminal taxa. *= accepted as significant with alpha <0.05. º= Lithostrotia + *Antarctosaurus.*

Table 9. Results of ancestor-descendant pairwise comparisons for shape PC3 in macronarian sauropods in our time-calibrated supertree (17 terminal taxa). n = ingroup internal nodes + terminal taxa. *= accepted s significant with alpha <0.05. º= Lithostrotia + *Antarctosaurus.*

TABLES

Table 1. Specimen sample used in this study. Proximodistal hind limb length measured in mm.

	Clade	Hind limb_length (mm)
Aeolosaurus	Aeolosaurini	1839
Ampelosaurus	Lirainosaurinae	1411
Antarctosaurus	Titanosauria	2351
Bonatitan	Lithostrotia	963
Bonitasaura	Lithostrotia	1987
Dreadnoughtus	Titanosauria	3184
Euhelopus	Euhelopodidae	1683
Jainosaurus	Titanosauria	2188
Ligabuesaurus	Somphospondyli	2866
Lirainosaurus	Lirainosaurinae	1074
Lohuecotitan	Lithostrotia	1120
Magyarosaurus	Lithostrotia	750
Mendozasaurus	Colossosauria	2334
Muyelensaurus	Colossosauria	1450
Neuquensaurus	Saltasauridae	1200
Oceanotitan	Macronaria	1892
Saltasaurus	Saltasauridae	1230

Table 2. PCA results over GPA aligned coordinates. Variance explained by each shape PC.

	Explained variance (%)	Cumulative variance (%)
PC1	29.92	29.92
PC2	14.83	44.75
PC3	11.61	56.36
PC4	8.83	65.19
PC5	7.02	72.21
PC6	6.09	78.3
PC7	4.18	82.48
PC8	3.75	86.23
PC9	3.12	89.35
PC10	2.19	91.53
PC11	2.15	93.68
PC12	1.95	95.64
PC13	1.56	97.19
PC14	1.18	98.38
PC15	0.92	99.29
PC16	0.71	100

Table 3. Kruskal-Wallis test on shape PCA variables between the most inclusive subclades analysed.

	Chi-sq	p-value	p-adjusted
PC1	11.954	0.153	1
PC2	5.592	0.693	1
PC3	7.886	0.445	1
PC4	9.647	0.291	1
PC5	5.17	0.739	1
PC6	7.618	0.472	1
PC7	8.915	0.35	1
PC8	8.941	0.347	1

PC9	10.206	0.251	1
PC10	10.422	0.237	1
PC11	4.768	0.782	1
PC12	5.66	0.685	1
PC13	8.886	0.352	1
PC14	9.856	0.275	1
PC15	10.248	0.248	1
PC16	4.578	0.802	1

Table 4. Phylogenetic ANOVA test on shape PCA variables between the most inclusive subclades studied.

		Df	SS	MS	R^2	F	Z	Pr(>F)
PC1	~Clade	8	0.073	0.009	0.466	0.872	-0.105	0.531
	Residuals	8	0.083	0.010	0.533	-	-	-
	Total	16	0.157	-	-	-	-	-
PC2	~Clade	8	0.001	1.50E+04	0.685	0.218	0.573	0.313
	Residuals	8	5,52E+04	6.90E+09	0.314	-	-	-
	Total1	16	0.002	-	-	-	-	-
PC3	~Clade	8	1.54E+04	1.93E+09	0.285	0.399	-0.925	0.82
	Residuals	8	3.86E+04	4,83E+08	0.714	-	-	-
	Total	16	5.40E+04	-	-	-	-	-
PC4	~Clade	8	1.49E+04	1.87E+09	0.3534	0.546	-0.496	0.658
	Residuals	8	2.73E+04	3,41E+09	0.646	-	-	-
	Total	16	4.22E+04	-	-	-	-	-
PC5	~Clade	8	3.77E+04	4,72E+09	0.556	125.362	0.121	0.452
	Residuals	8	3.01E+04	3,77E+09	0.443	-	-	-
	Total	16	6.79E+04	-	-	-	-	-
PC6	~Clade	8	3.24E+04	4,06E+09	0.590	144.158	0.590	0.264
	Residuals	8	2.25E+04	2,82E+09	0.409	-	-	-
	Total	16	5.50E+04	-	-	-	-	-
	~Clade	8	1.63E+04	2,05E+09	0.434	0.768	-0.315	0.625
	Residuals	8	2.13E+04	2,66E+09	0.565	-	-	-
	Total	16	3.76E+04	-	-	-	-	-

Table 5. RMA models of the shape PCs against log-transformed Centroid size. CI – confidence interval.

	intercept	slope	CI 2.5% Slope	CI 97.5% Slope	r^2	P
PC1	0.221	-0.102	-0.168	-0.062	0.105	0.204
PC2	0.155	-0.072	-0.12	-0.043	0.054	0.371
PC3	0.137	-0.064	-0.106	-0.038	0.055	0.363
PC4	0.12	-0.055	-0.093	-0.033	0.026	0.534
PC5	-0.107	0.049	0.03	0.082	0.079	0.275
PC6	-0.1	0.046	0.028	0.076	0.086	0.254

Table 6. Estimated phylogenetic signal via Pagel's lambda. *p* value of log-likelihood ratio test after 1000 simulations. * Indicates significant relationships for an alpha of 0.05. log-Csize – Log-transformed hind limb centroid size.

	Lambda	p
log-Csize	0.982	0.003*
PC1	0.715	0.000*

PC2	0	1
PC3	0.76	0.002*
PC4	0	1
PC5	0.778	0.031*
PC6	0.697	0.01*

Table 7. Results of pairwise ancestor-descendant comparisons for log-transformed centroid size in macronarian sauropods in our time-calibrated supertree (17 terminal taxa). n = ingroup internal nodes + terminal taxa. *= accepted as significant with alpha <0.05. º= Lithostrotia + *Antarctosaurus*.

Clade	Mean	Sum	Skew	Median	n	Positive changes	Negative changes	χ^2	p
Titanosauriformes	-0.127	-3.819	-0.223	-0.032	30	12	18	1.2	0.273
Somphospondyli	-0.366	-10.252	-0.148	-0.256	28	4	24	14.286	0.000*
Titanosauria	-0.288	-7.488	-0.088	-0.182	26	5	21	9.846	0.002*
Lithostrotiaº	-0.283	-6.22	-0.193	-0.307	22	5	17	6.545	0.011*

Table 8. Results of ancestor-descendant pairwise comparisons for shape PC1 in macronarian sauropods in our time-calibrated supertree (17 terminal taxa). n = ingroup internal nodes + terminal taxa. *= accepted as significant with alpha <0.05. º= Lithostrotia + *Antarctosaurus*.

Clade	Mean	Sum	Skew	Median	n	Positive changes	Negative changes	χ^2	p
Titanosauriformes	0.051	1.518	0.98	0.043	30	29	1	26.133	0.000*
Somphospondyli	0.019	0.538	1.158	0.012	28	20	7	6.259	0.012*
Titanosauria	0.011	0.291	1.076	0.003	26	14	10	0.667	0.414
Lithostrotiaº	0.011	0.24	1.079	0.002	22	11	10	0.048	0.827

Table 9. Results of ancestor-descendant pairwise comparisons for shape PC3 in macronarian sauropods in our time-calibrated supertree (17 terminal taxa). n = ingroup internal nodes + terminal taxa. *= accepted s significant with alpha <0.05. º= Lithostrotia + *Antarctosaurus*.

Clade	Mean	Sum	Skew	Median	n	Positive changes	Negative changes	χ^2	p
Titanosauriformes	-0.03	-1.04	1.697	-0.038	30	2	28	22.533	0.000*

	5	7							
Somphospondyli	-0.023	-0.639	2.174	-0.024	28	2	26	20.571	0.000*
Titanosauria	-0.008	-0.21	2.483	-0.009	26	3	23	15.385	0.000*
Lithostrotia°	-0.003	-0.074	2.323	-0.004	22	4	17	8.048	0.005*

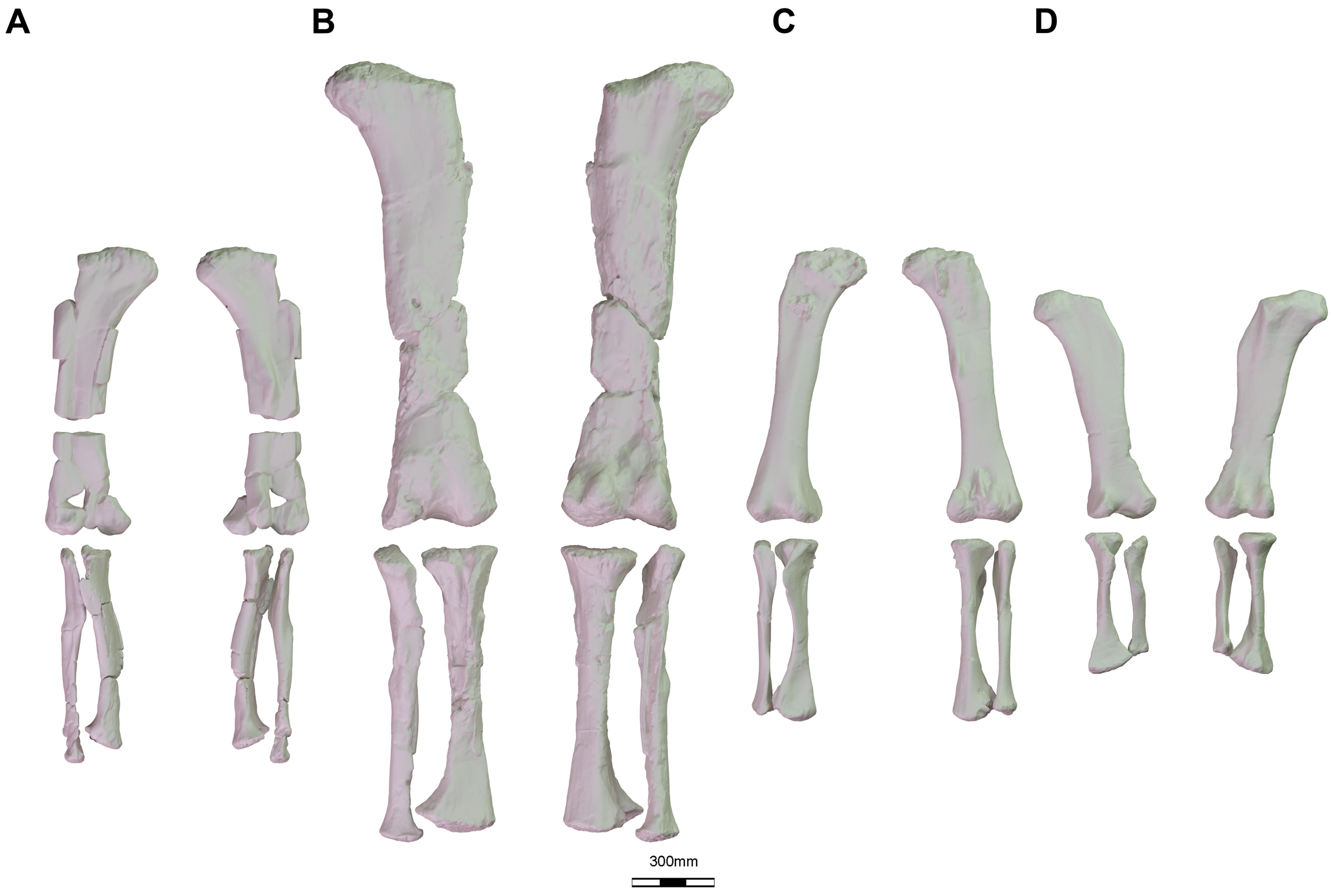
A
B
C
D
300mm

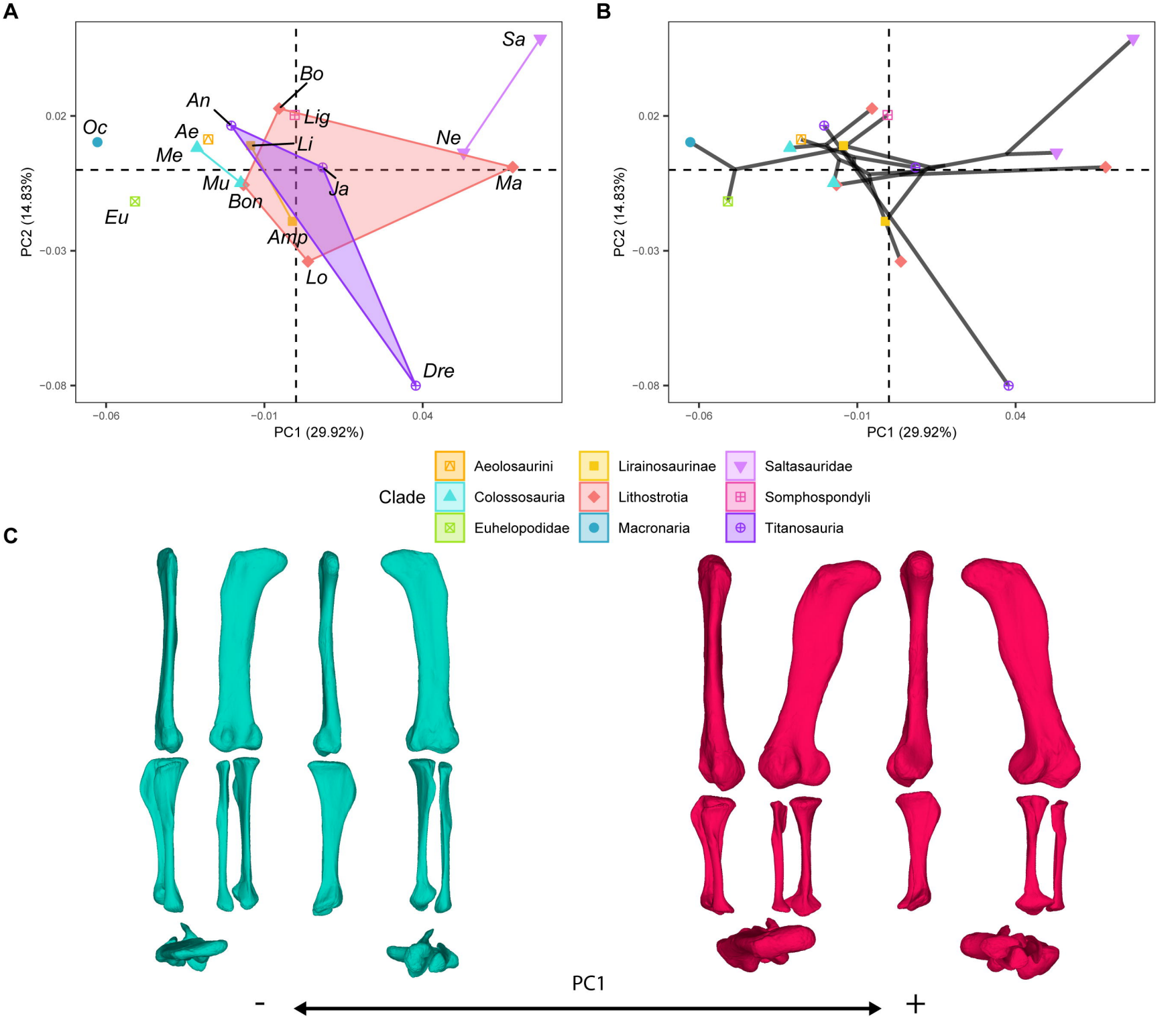
A
B
C
Sa
Bo
An
Lig
Oc
Ae
Li
Ne
Me
Mu
Ja
Ma
Bon
Eu
Amp
Lo
Dre
0.02
−0.03
−0.08
−0.06
−0.01
0.04
PC1 (29.92%)
PC2 (14.83%)
Clade
Aeolosaurini
Colossosauria
Euhelopodidae
Lirainosaurinae
Lithostrotia
Macronaria
Saltasauridae
Somphospondyli
Titanosauria
PC1
-
+

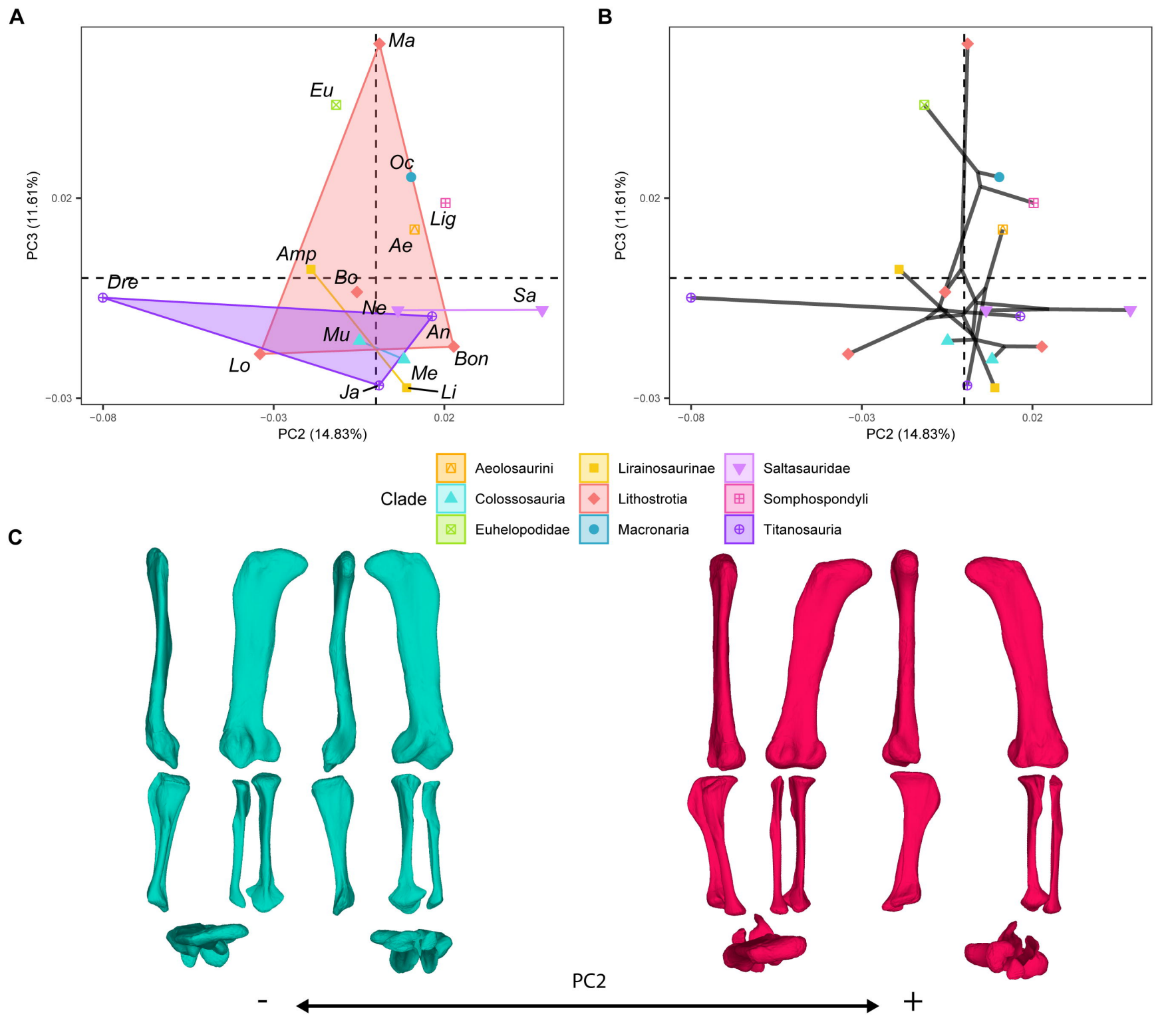
A
B
C
Ma
Eu
Oc
Lig
Ae
Amp
Bo
Dre
Sa
Ne
Mu
An
Bon
Lo
Me
Ja
Li
PC3 (11.61%)
PC2 (14.83%)
0.02
−0.03
−0.08
−0.03
0.02
Clade
Aeolosaurini
Colossosauria
Euhelopodidae
Lirainosaurinae
Lithostrotia
Macronaria
Saltasauridae
Somphospondyli
Titanosauria
PC2
-
+

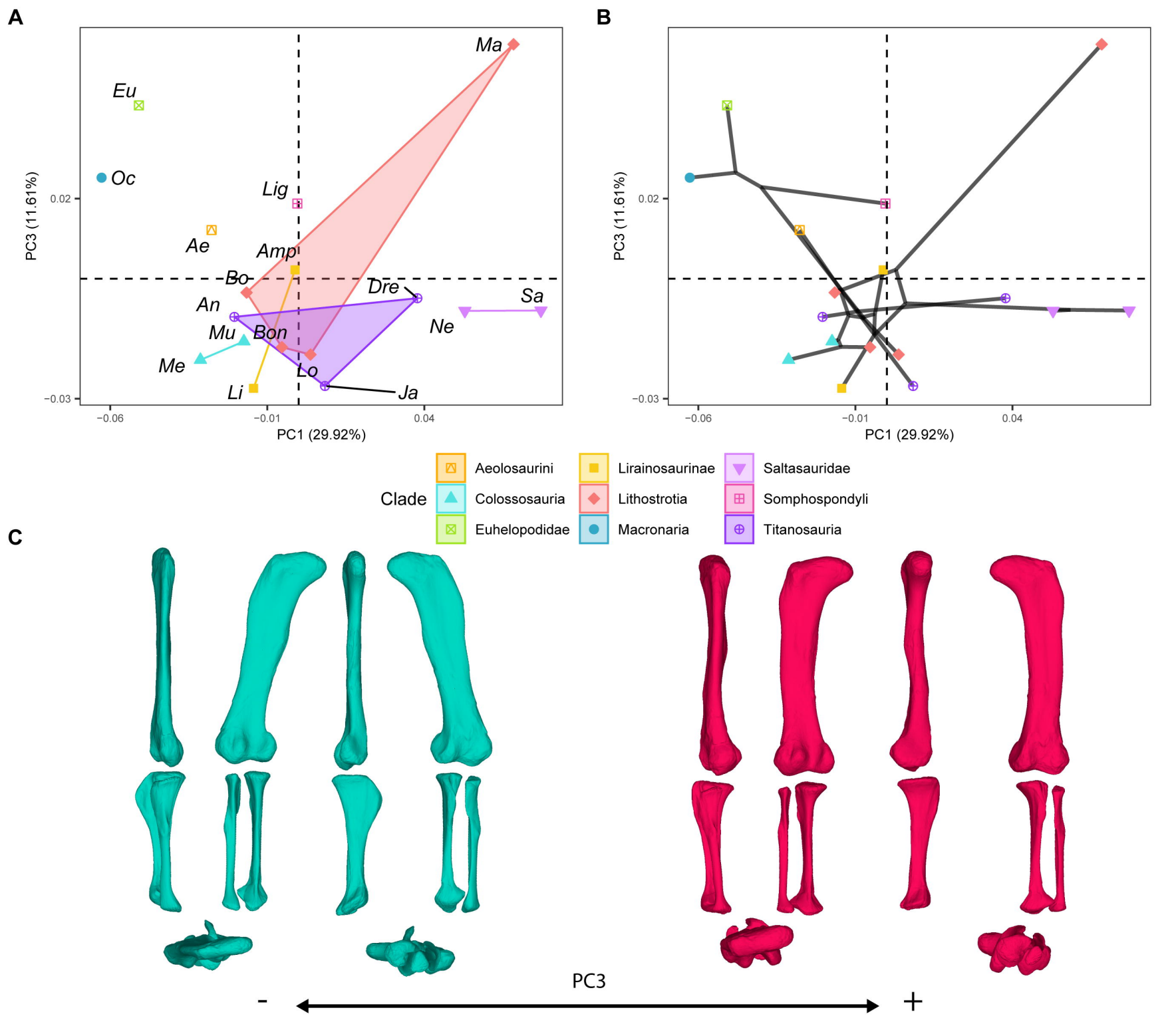
A
B
C
Ma
Eu
Oc
Lig
Ae
Amp
Bo
Dre
Sa
An
Mu
Bon
Ne
Me
Lo
Li
Ja
PC3 (11.61%)
PC1 (29.92%)
0.02
−0.03
−0.06
−0.01
0.04
Clade
Aeolosaurini
Colossosauria
Euhelopodidae
Lirainosaurinae
Lithostrotia
Macronaria
Saltasauridae
Somphospondyli
Titanosauria
PC3
-
+

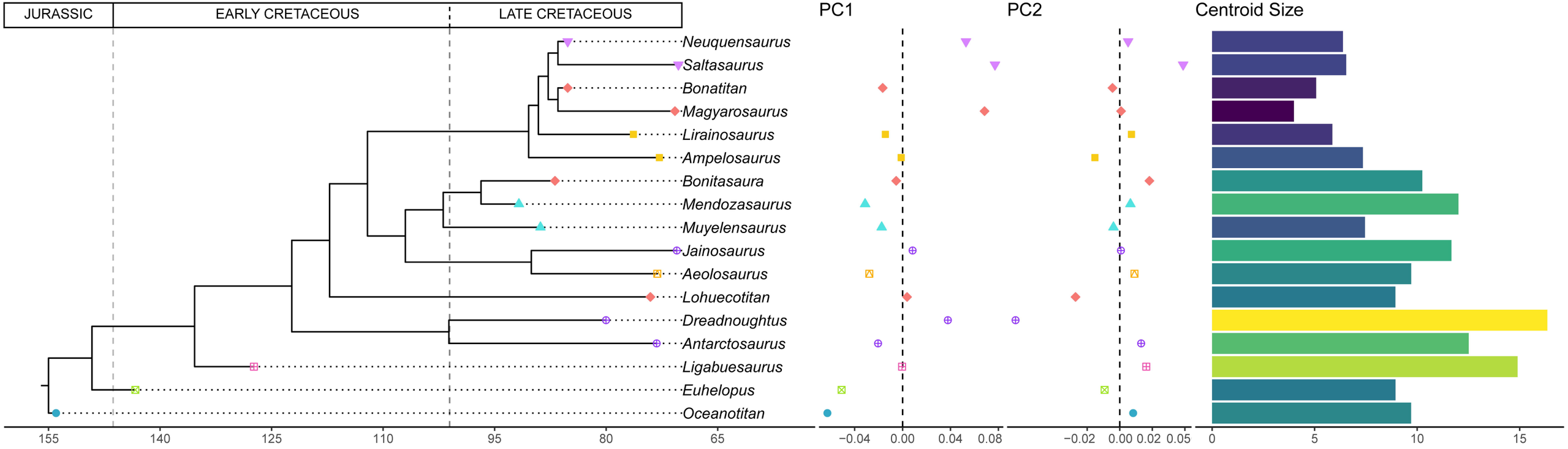
JURASSIC
EARLY CRETACEOUS
LATE CRETACEOUS
PC1
PC2
Centroid Size
Neuquensaurus
Saltasaurus
Bonatitan
Magyarosaurus
Lirainosaurus
Ampelosaurus
Bonitasaura
Mendozasaurus
Muyelensaurus
Jainosaurus
Aeolosaurus
Lohuecotitan
Dreadnoughtus
Antarctosaurus
Ligabuesaurus
Euhelopus
Oceanotitan
155
140
125
110
95
80
65
−0.04
0.00
0.04
0.08
−0.02
0.00
0.02
0.05
0
5
10
15

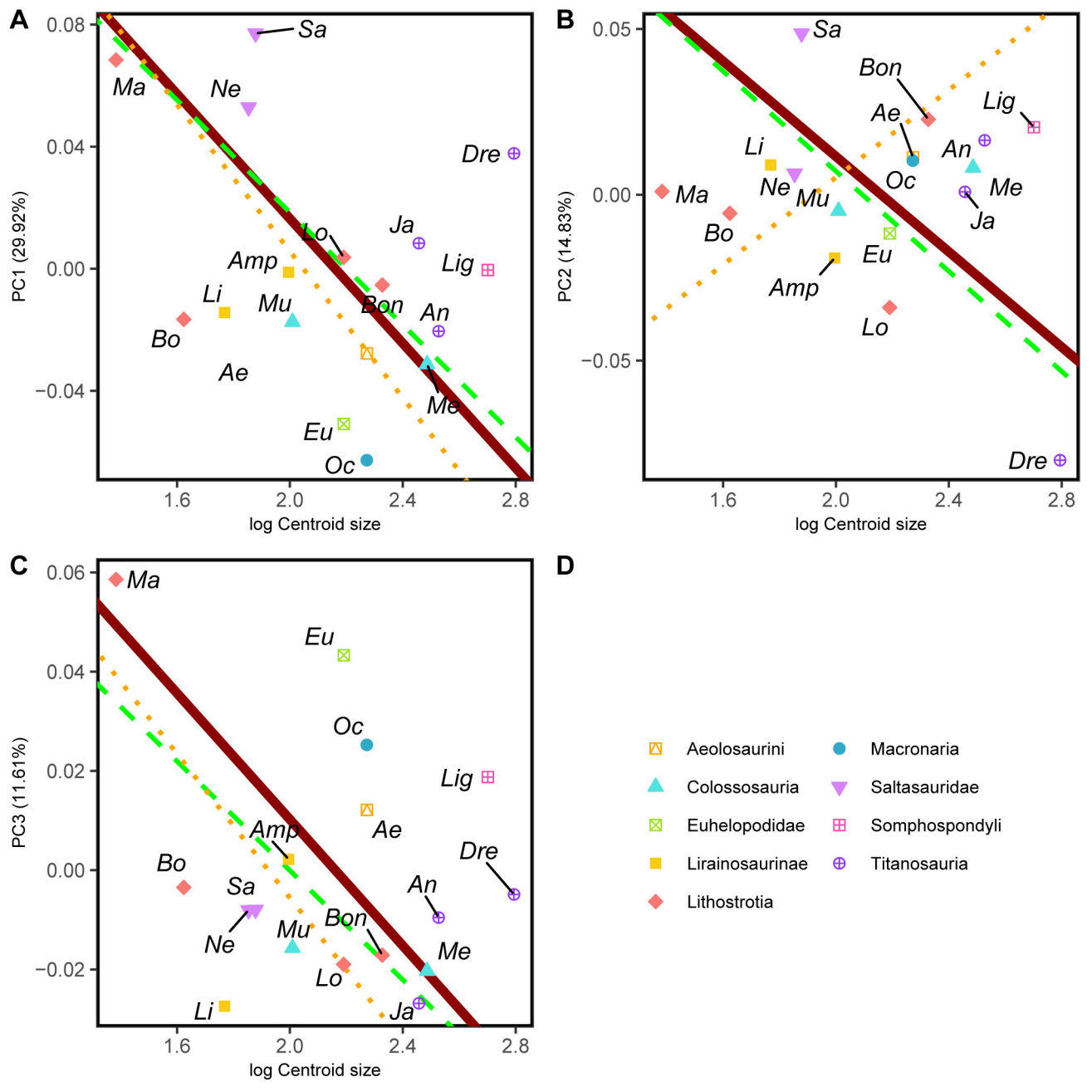
A
PC1 (29.92%)
log Centroid size
Sa
Ma
Ne
Dre
Ja
Lo
Amp
Lig
Li
Mu
Bon
An
Bo
Ae
Me
Eu
Oc
B
PC2 (14.83%)
log Centroid size
Sa
Bon
Lig
Ae
Li
An
Oc
Ne
Me
Ma
Mu
Ja
Bo
Eu
Amp
Lo
Dre
C
PC3 (11.61%)
log Centroid size
Ma
Eu
Oc
Lig
Amp
Ae
Dre
Bo
Sa
An
Bon
Mu
Ne
Me
Lo
Li
Ja
D
Aeolosaurini
Colossosauria
Euhelopodidae
Lirainosaurinae
Lithostrotia
Macronaria
Saltasauridae
Somphospondyli
Titanosauria

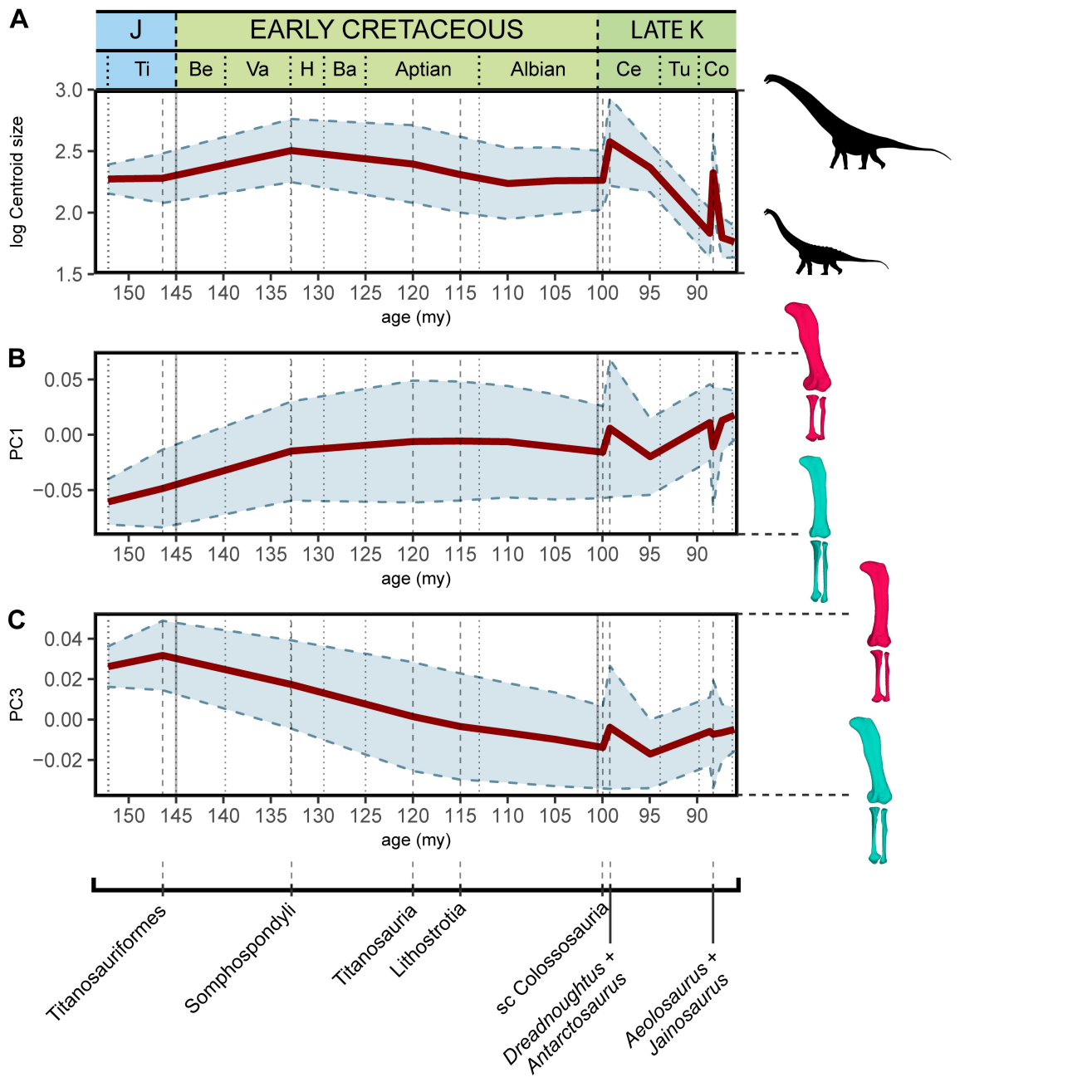
A
J
EARLY CRETACEOUS
LATE K
Ti
Be
Va
H
Ba
Aptian
Albian
Ce
Tu
Co
log Centroid size
3.0
2.5
2.0
1.5
150 145 140 135 130 125 120 115 110 105 100 95 90
age (my)
B
PC1
0.05
0.00
−0.05
150 145 140 135 130 125 120 115 110 105 100 95 90
age (my)
C
PC3
0.04
0.02
0.00
−0.02
150 145 140 135 130 125 120 115 110 105 100 95 90
age (my)
Titanosauriformes
Somphospondyli
Titanosauria
Lithostrotia
sc Colossosauria
Dreadnoughtus +
Antarctosaurus
Aeolosaurus +
Jainosaurus